Artificial neural network for Gaussian and non Gaussian random fatigue loading analysis

J F Durodola*

Oxford Brookes University, Faculty of Technology, Design and Environment, Wheatley Campus, Oxford OX33 1HX, UK.

Abstract

There has been a lot of work done on the analysis of Gaussian loading analysis perhaps because its occurrence is more common than non-Gaussian loading problems. It is nevertheless known that non Gaussian load occur in many instances especially in various forms of transport, land, sea and space. Part of the challenge with non Gaussian loading analysis is the increased number of variables that are needed to model the loading adequately. Artificial neural network (ANN) approach provide a versatile means to develop models that may require many input variables in order to achieve applicable predictive generalisation capabilities. ANN has been shown to perform much better than existing frequency domain methods for random fatigue loading under stationary Gaussian load forms especially when mean stress effects are included. This paper presents an ANN model with greater predictive capability than existing frequency domain methods for both Gaussian and non Gaussian loading analysis. Both platykurtic and leptokurtic non Gaussian loading cases were considered to demonstrate the scope of application. The model was also validated with available SAE experimental data even though the skewness and kurtosis of the signal in this case were mild.

Keywords non Gaussian, random fatigue, frequency, time domain, artificial neural networks, Dirlik

*Corresponding author, email: jdurodola@brookes.ac.uk; Tel: + 44 (0)1865 483501.

1. Introduction

Stationary ergodic Gaussian random data has been the convenient basis of many of the data used for the development of models for the analysis of random vibration fatigue problems especially using spectral based methods [1-5]. It is however known that non Gaussian excitations occur due to road irregularities in automobiles, and turbulent pressure flections in the aerospace sector [6, 7]. Highly non Gaussian excitations occur on rail vehicles caused by wheel rail contact [8]. Wind loading effects are also known to be non Gaussian with high uncertainties and peak values [9]. The main consequence of non Gaussian data effect is that its peakedness effect can be overlooked in analysis and lead to failure. There have, therefore, been a lot of interest in non Gaussian fatigue loading analysis [7, 10]. A number of researchers have attempted to use higher order statistical properties such as signal Kurtosis as an additional parameter to resolve issues associated with inaccuracies encountered in fatigue life prediction under non Gaussian loading condition [11] A lot of effort has also been going on towards the modelling simulation of non Gaussian data for fatigue analysis[7, 10, 12, 13].

Various methods have been proposed for the simulation or generation of non Gaussian data or its development for analysis purposes. An approach for the simulation of non Gaussian data uses zero-memory nonlinear (ZMNL) monotonic function to convert a zero mean Gaussian signal x(t) with a specified PSD into a non-Gaussian waveform y(t)[7, 10]. This approach is also known as the PDF transform technique [10]. Smallwood presented three ZMNL function based methods for the transformation [7]. In one method, a six parameter function was proposed with an error objective function that is based on a specified skewness and Kurtosis values. This was then solved using optimisation method to determine the function parameters. A second method was based on a cubic polynomial function. The function parameters were also determined using optimisation solvers. The third method based on Hermite polynomial method was solved by Winterstein [14] to obtain a closed form solution in terms of specified skewness and Kurtosis values. This formula worked for leptokurtic signal with Kurtosis value > 3.

Winterstein also presented a closed form solution for platykurtic signal with a value < 3. Yet another approach of generating non Gaussian signal is by modulating a stationary Gaussian signal[10]. The modulating signal is made up of a burst, which is in the form of a wave and followed by a passive steady factor part. It is helpful to note in passing that a Gaussian distribution has a kurtosis value of 3 and a skewness value of zero [15-17]. There have also been alternative methods for the treatment of non Gaussian data. One of such methods is known as Random Gaussian Sequence Decomposition (RGSD) method. This method effectively decomposes the non Gaussian data into Gaussian distributed parts [8, 13] before subsequent use for fatigue damage prediction. Some attempts have been made to account for the effect on non Gaussianity in fatigue calculations. Most of the effort has been directed at determining a correction factor that will allow the non Gaussian load damage to be determined by applying a correction factor to the damage obtained based on the consideration of the associated baseline Gaussian load [18-21]. The challenge with these methods is that the inversion process to determine the Gaussian signal associated with a non Gaussian signal is fraught with limitations and constraints. Although there are inversion formulas in certain cases [14, 21], these do not guarantee that the inverted Gaussian signals obtained are practically meaningful in all cases. Another factor in random data fatigue analysis that is of concern is non stationarity in which case the time shift invariance of the signal does not exist, i.e. $E[x(t)] \neq E[x(t+\tau)]$. This problem is not considered in the present study.

There have been a lot of interest in the use of ANN for fatigue characterisation over the past two decades as can be seen in references [22-26]. These references aimed to use ANN to relate stress amplitude with life, predict crack propagation rate, identify fatigue spectral load types, develop cumulative damage relationships for materials and the study of the effect of stress ratio. Kim et al [26] suggested the coupling of stress range or amplitude probability distribution functions for random fatigue loading such as those in references [1, 27-29] with the spectral identification carried out using ANN.

The author together with colleagues [30] uniquely proposed the use of ANN as a general tool for a wide scope of spectral loading covering a broad range of conceivable metal alloys. Stationary zero mean Gaussian signals were covered in the first instance; this was followed by ANN models which cover globally non zero mean stress signals[31]. As highlighted in the foregoing, non Gaussian loading cause more damage because of burst effects than zero mean stationary Gaussian data. One of the challenges with non Gaussian analysis that still requires attention is the development of models that are capable of accounting for the effects of the wider variability in the form of the data compared to Gaussian data.

The ability of ANN to provide predictive generalization involving non-linear relationship and a number of parameters has been one of the strengths of the method [32]. This potential has been explored and utilized by the author and colleagues in solving a few problems [33-36]. This paper models Gaussian and non Gaussian stationary data to demonstrate the capabilities of ANN to analyse these types of data as a general random fatigue analysis method. Platykurtic and, leptokurtic data were investigated. The method uses a combination of rainflow counting time method together with a combination of spectral parameters and easily extracted time data as inputs for the ANN. This allows a generalisation that is not possible with the use of spectral based methods only. The materials considered in this work are metallic alloys. The aim of this work as with past works by the author and colleagues is to obtain predictive generalization using ANN over a broad range of material properties, component conditions and various spectral types for random fatigue loading analysis.

2. Gaussian and non Gaussian signal generation

Stationary zero mean Gaussian data can be directly modelled using (1) [4, 37]. For every combination of spectra parameters, the corresponding Gaussian time domain signal for the selected spectrum was generated using equation (1) [37],

$$x_n(t) = \sum_{k=1}^{N} [2G_x(f_k)\Delta f]^{1/2} [\cos(2\pi f t + \phi_{k,n})] \quad (1)$$

where n is the sample number, N is the number of discretisation of the power spectral density G_x that underlies the signal; with $f_k = (k - 0.5)\Delta f$ and $\phi_{k,n}$ are mutually independent random phase angles distributed uniformly over the range 0 to 2π [16]. The characteristics of the peak values in this signal is that they follow the Gaussian probability distribution function described in equation (2) [16],

$$f(x \mid \mu, \sigma^2) = e^{-\frac{(x-\mu)^2}{2\sigma^2}} / \sqrt{2\pi\sigma^2} \quad (2)$$

where μ and σ are the mean and standard deviation of the signal. It is helpful at this stage to introduce the skewness, S_k, and the kurtosis, K_r, of a signal, which will be needed for the description of non Gaussian, signals. These are given by equations (3) and (4) [17]

$$S_k(x) = E\left[\left(\frac{x-\mu}{\sigma}\right)^3\right] \quad (3)$$

$$K_r(x) = E\left[\left(\frac{x-\mu}{\sigma}\right)^4\right] \quad (4)$$

where the letter E is used to describe the statistical expectation of the quantity in the bracket. The skewness and the kurtosis describe the asymmetry and spread or tailedness of the signal respectively. The values of these parameters are 0 and 3 for Gaussian distribution functions[10, 15].

As highlighted in the foregoing, many fatigue loading distribution do not necessarily follow the Gaussian distribution. There have been a number of attempts to model or generate non Gaussian fatigue loading signal distributions using different methods. Some signals including burst types are described by for example beta distribution [7, 10]. The probability distribution function for the beta function is given by equation (5) [38].

$$f(x|u, v, p, q) = \frac{(x-u)^{p-1}(v-x)^{q-1}}{B(p,q)(v-u)^{p+q-1}} \quad (5)$$

$$u \le x \le v; \quad p, q > 0$$

where p and q are shape parameters that determine the skewness and kurtosis values respectively, u and v are the lower and upper bounds of the signal x respectively. *B(p,q)* is beta function given by equation (6).

$$B(p,q) = \int_0^1 r^{p-1}(1-r)^{q-1}dr \tag{6}$$

where *r* varies between 0 and 1. The cumulative beta probability function at a probability of r' is given by equation (7) [38]

$$I_{r'}(p,q) = \frac{\int_0^{r'} r^{p-1}(1-r)^{q-1}dr}{B(p,q)} \tag{7}$$

wherein *r'* ranges from 0 to 1. Following from the expressions in reference [17], the specific values of *p* and *q* that correspond to the desired or required values of the skewness, S_k , and the kurtosis, K_r can be obtained by solving the non linear equations (8) and (9) as carried out in this work.

$${S_k}^2 = \frac{4(q-p)^2(p+q+1)}{pq(p+q+2)^2} \tag{8}$$

$$K_r - 3 = \frac{6[(p-q)^2(p+q+1)-pq(p+q+2)]}{pq(p+q+2)(p+q+3)} \tag{9}$$

Using similar approach as in Lalanne [16], a beta distribution signal can be generated by using equation (1) but with the phase array term given by equation (10).

$$\phi = 2\pi I_{r'}(p,q) \tag{10}$$

The *r* value in equation (7) is to be selected from a uniformly distributed random number between 0 and 1. The signal *x(t)* generated in this way preserves the shape of the power spectral density G_x approximately. An alternative iterative shuffling algorithm based on memoryless nonlinear transformation approach presented by Nichols et al [12] achieves closer spectral density shape preservation for any chosen probability distribution function than direct application of equations (1) to (8). The method first determines the spectral amplitudes from the desired power spectral density function, G_x, and then shuffles this iteratively to match the target non Gaussian distribution function and subject to the preservation of the variance of the PSD. The target distribution function can be of the form of beta, Rayleigh or any desired

function. The shuffling method as to be expected and of course takes longer time relatively to generate the non-Gaussian data.

A leptokurtic non Gaussian signal *y(t)* can be obtained by applying the Winterstein formula [14] given here as equation (11)

$$y(t) = \mu_x + \sigma_x J\left[\frac{x}{\sigma_x} + \overline{h_3}\left(\frac{x}{\sigma_x} - 1\right) + \overline{h_4}\left(\left(\frac{x}{\sigma_x}\right)^3 - 3\frac{x}{\sigma_x}\right)\right] \tag{11}$$

with

$$J = \frac{1}{\sqrt{1 + 2\bar{h}^2 + 6\overline{h_4}^2}};\quad \overline{h_3} = \frac{S_k}{6(1 + 6\overline{h_4})};\quad \overline{h_4} = \frac{\sqrt{1 + 1.5(K_r - 3)} - 1}{18} \tag{12}$$

where S_k and K_r a are the expected skewness and kurtosis respectively and where *x* is a Gaussian signal based on a given spectral density G_x. This model appears to be widely accepted and known to provide an accurate representation of a wide range of nonlinear behaviours[10].

For the purpose of the presentations in this work, five different types of signals were considered and denoted as *T0,T1,T2, T3 and T4* , . *T0* is used to denote a Gaussian distribution signal with globally zero mean stress, *T1* is used to denote a Gaussian distribution signal with generally globally non zero mean stress. *T2* is used to describe the signals generated using the direct generation of non Gaussians by use of appropriate phase selection as given in equations (10) and (1) [16]. The signals generated using the leptokurtic equation (11) developed by Winterstein [14] is referred to as *T3.* The method of power spectral amplitude shuffling [12] described in the foregoing was used to generate the signals denoted as *T4.*

In all the signals generated, the maximum signal frequency f in equation (1) was 200 Hz. In the analyses carried out, the sampling frequency used to evaluate the power spectral density $G_x(f)$ was varied between 400 to 6.4 kHz [39]. All signals *T1* to *T4* were randomly shifted in

the stress space so as to include signals with globally non zero mean stress. The signal *x(t)* was however scaled to lie within 5 to 94% of the ultimate strength of the test material so as to achieve fatigue rather monotonic failure. The global mean stress of the signal *x(t)* was within $\pm$ 60% of the ultimate tensile strength.

3 Frequency domain fatigue damage analysis

The ANN method proposed uses both frequency and time domain parameters. Many of the inputs used as highlighted in section 4 of this paper are based on frequency domain parameters for characterising signals. The primary ones are the spectral moments, which are obtained from the power spectral density (PSD) of the signal as highlighted in equation (13).

$$m_i = \int_0^\infty f^i G_x(f) df \tag{13}$$

where m_i is the i th moment of the PSD $G_x(f)$ of the signal The moments used in the Dirlik[1] formulation are given by i = 0, 1, 2, 4 for fatigue loading characterisation. Also significant are the estimates for the number of mean crossing *E(0*) and peaks *E(P)* per second, which are given by equations (14) and (15). From these two numbers, the irregularity factor, γ, of the signal is obtained using equation (16).

$$E(0) = \left(m_2 / m_0\right)^{1/2} \tag{14}$$

$$E(P) = \left(m_4 / m_2\right)^{1/2} \tag{15}$$

$$\gamma = E(0)/E(P) = m_2 / \left(m_0 m_4\right)^{1/2} \tag{16}$$

The irregularity factor gives an indication of the breadth of the frequency content of the signal. A value of γ tending to 0 represents a narrow band signal while 1 suggests a broad band signal.

3.1 Damage calculation

The calculation of damage was carried out using both time domain and frequency domain methods. The time domain damage calculation produced data for the output as target values for the ANN training. The frequency domain damage calculation was carried for comparison purposes. The Basquin's stress life equation and the Miner's linear cumulative damage rule [40] for different fatigue loading states are involved in both cases. For a given load – life state (S_{ai}, S_{mi} *and* n_i), the Basquin's equation with mean stress correction is expressed as in equations (17) and (18),

$$S_{ai} = \alpha_i \, a \, N_i^b \tag{17}$$

$$\alpha_i = (1 - S_{mi} / S_u) \tag{18}$$

in these, S_{ai}, S_{mi} and n_i are the amplitude, the mean stress and number of cycles representing the loading corresponding to the state *i* and *a* and *b* are the fatigue mechanical properties of the component which includes material and all influencing factors such as load type, dimension, surface finish and stress concentration factors. The effect of mean stress is accounted for by the α_i parameter. The Goodman's method [40] is used in equation (18). The ultimate strength of the material is represented as S_u. If under this state, N_i is the maximum number of cycles possible, the Miner's rule for cumulating the damage for all occurring states *i is* as given in equation (19)

$$E(D) = \sum_i n_i / N_i \tag{19}$$

N_i is obtained using equations (17) and (18).

The damage calculation in the frequency domain approach was carried using equation (20). It should be noted that the Miner's rule is inherent in this equation.

$$E(D) = E(P)\frac{T}{k}\int_0^\infty S^v p(S) dS \tag{20}$$

In equation (20), *T* is the time taken for the sampling of the signal and *S* is the stress range variable. The parameters *v* and *k* are related to *a* and *b* as being equal to *-1/b* and $(2a)^{-1/b}$ respectively. The probability distribution of the stress range is represented as *p(S)* in (20). The probability distribution function derived by Dirlik [1] which is given here in equation (21) has been widely applied in the literature for broadband signal fatigue problems.

$$p(S) = \left[\frac{D_1}{Q} e^{-Z/Q} + \frac{D_2 Z}{R^2} e^{-Z^2/2R^2} + D_3 Z e^{-Z^2/2} \right] / 2m_o^{1/2} \tag{21}$$

In (21), Z is a function of the stress range and the spectral moment m_0. The parameters *R, Q,* D_1, D_2 and D_3 are all function of the spectral moments m_i, *i=0,1,2* and *4.*

For non Gaussian loading fatigue damage determination, a correction factor approach has been proposed by a number of authors, for example Bracessi et al[41]. In applying this method, first the baseline Gaussian signal corresponding to the non Gaussian signal is determined. Then, the damage for the Gaussian signal is determined and the correction factor is the applied to this in order to obtain the non Gaussian fatigue loading data. The equation proposed by Bracessi that takes both the skewness and kurtosis into account is given in equation (22).

$$E(D_{nG}) = \lambda_{nG} E(D_G) \tag{22}$$

where λ_{nG}, $E(D_G)$ and $E(D_{nG})$ are the correction factor, damage for the Gaussian and non Gaussian data respectively. The correction factor equation developed by Bracessi et al, which appears to be well cited, is given in equation (23).

$$\lambda_{nG} = \exp\left[\frac{m^{3/2}}{\pi} \left(\frac{K_r - 3}{5} - \frac{S_k^2}{4} \right) \right] \tag{23}$$

where m which is related to the fatigue exponent is = *-1/b*.

4 ANN model

This section presents an outline of the bases and methods used for the ANN model presented here. The structure of the ANN used, the types of signals considered, the input-output parameters used, the numerical training, validation and testing of the model is highlighted in this section.

4.1 ANN architecture

Three layers of neuron as illustrated in Figure 1 which is generally accepted as sufficient to represent any non-linear function approximation [18] was used as the architecture of the ANN. Various numbers of input were considered in the study. The input parameters considered are presented in section 4.2. The number of hidden layer used was 25 as in previous studies [30, 31]. This number was found to be adequate by checking the residual error and goodness of fit of the ANN prediction with target results. The result from the single output neuron was the logarithmic value of the fatigue damage. In order to study the effect of the density of the coverage of the sampling space, the numbers of signals constructed and tested ranged from 100 to 50,000.

4.2 ANN Input - output

The input and output parameters used in the study are listed in this section. The input parameters include fatigue material properties, a and b and the ultimate tensile strength, S_u ; seven spectral moments m_i, $i = 0,6;$ the Goodman parameter α_m; a mean complementary parameter $\alpha_c = 1 - \alpha_m$; and two crest parameters γ_p and γ_n. The crest parameters were equal to the ratios of maximum and minimum stress in the signal to the ultimate tensile strength of the material respectively. The other input parameters used include the skewness S_k and kurtosis K_r. These parameters are listed symbolically as: $m_{i,\, i=0,6}, a,\ b,\ S_u, \alpha_m,\ \alpha_c,\ \gamma_p, \gamma_n,\ S_k,\ K_r$ where

$$\alpha_m = \left(1 - \frac{S_m}{S_u}\right) \quad \text{for } S_m > 0 \tag{24}$$

$$\alpha_m = 1 \quad \text{for } S_m < 0 \tag{25}$$

and $\alpha_c = {}^{S_m}/_{S_u}$; $\gamma_n = {}^{S_{min}}/_{S_u}, \gamma_p = {}^{S_{max}}/_{S_u}$; where S_{min} and S_{max} are the minimum and maximum values of x.

Four different types of input sets were considered for the implementation of the artificial neural network model. These are listed in Table 2 as *N1, N2, N3* and *N4* models. *N1* is a model based on the inputs identified in a previous work as being necessary in order to obtain good predictions for Gaussian fatigue load with mean stress. Model *N2* additionally includes the skewness, S_k , and the kurtosis, K_r , parameters. This was considered because of the additional variability that occurs in non Gaussian data compared to Gaussian data. Model *N3* adds the spectral moment m_3 in case *N2* should prove to be inadequate to generalize fatigue life prediction for non Gaussian signal. Since the kurtosis is a fourth order moment, additional spectral moments up to the sixth order, i.e. m_5 and m_6 were added to *N3* for the model *N4*.

The target damage E(D) were taken as the values obtained using the rainflow counting time domain method [42]. Although the method does not have consistent convergence characteristics relative to experimental results [31], it is still the most acclaimed method for time domain cycle counting damage calculation [40]. The logarithmic value of the damage E(D) was used as the output target value. This approach helped to reduce the impact of the spread of the damage values, which is normally broad by several orders.

4.3 Training, validation and testing of the ANN models

The training, validation and testing process followed in this work is similar to those in previous works by the author and colleagues[30, 31, 43]. Generally, the feed forward backpropagation multilayer perceptron (MLP) model was followed. The training starts by initialising the weights W_{ij} in the neuron connections illustrated in Figure 1. The output to a next layer is obtained by summing the products of the weights and the corresponding inputs. This sum is then transformed using an activation function [32] before being used as the input to the next layer. This feedforward process progresses through to the output layer where a comparison is then made between the calculated value and the expected target

value. The difference is an error that is used in the backpropagation process to modify or correct the weights in the next iteration. This approach is known as a supervised learning training method[32].

The output from an ANN does not in general match the known output corresponding to the inputs used from the data set, at least in the first feedforward through process. The mis-match error is a function of the weights associated with the neurons. The aim of the training is to determine the weights associated with the neurons that minimise the error. The minimisation process was carried out iteratively in many stages. Various error reduction backpropagation algorithms have been devised for the training of networks [44]. The implementation of the ANN in this work was carried out using a set of in-house routines developed in a MATLAB [25] environment together with the Levenberg Marquardt error backpropagation and weight correction method in the MATLAB ANN toolbox.

After experimenting with various proportions, the percentages of data finally used for training, validation and testing were 70, 15 and 15% respectively[30, 31]. The training process was based on 70% of the total data generated. A validation set which was 15% of the total number of signals, was used to independently check the performance of the ANN weights obtained in the training process. This was to ensure that the ANN model had not simply over fitted or memorised the relationship between the training data and the output but actually developed the capability to make a prediction for an unseen set of data. The validation set was used to detect when the tendency for overfitting was about to set in and the training process was stopped at this stage. The final 15% data set was used to provide an independent test of the ANN model. The data used in this process was different from the data used for the training and validation steps.

5 Overall procedure

The overall procedure of the work may be summarised as follows. Signal types *T0* to *T4* were randomly generated using the methods described in section 2. Up to 50,000 signals were generated for some studies. All parameters such as signal type, material properties, *PSD* form $G_x(f)$ and associated parameters were selected using Latin Hypercube Sampling [LHS] [45, 46] method to ensure broad coverage of the parameters. The target damage values corresponding

to the signals to be used for the ANN training were then calculated using the time domain rainflow counting and Miners rule methods[40, 42]. The parameters of the signals and the output target values were then used to train, validate and test the ANN. Various combinations of inputs were tested as indicated in section 4.2. The weights of the ANN obtained were then used to demonstrate the capabilities of the ANN as highlighted in section 6. The limits of the material properties, spectral moment values m_i, $i = 0,6$ and other signal characteristics considered in the work are highlighted in Table 2.

6. Results

This section highlights the form of the non Gaussian signals analysed and the results of the application of different types ANN models N1 to N4 to learn and to predict relationships for non Gaussian fatigue problems. The results obtained from ANN predictions are compared with those obtained using other methods. The performance of the ANN on SAE experimental data is also presented.

6.1 Skewness and kurtosis of signals

This section highlights the types of non Gaussian signals analysed. The signals were generated using the equations and methods described in section 2 of this work. Figure 2 shows four different types of signals with different skewness and kurtosis values. Figure 2(a) shows the stress history distributions and Figure 2(b) shows the corresponding histogram distributions. Figure 2(b) (i) through to (iii) can be seen to show higher values of outliers than Figure 2(b) (iv) for example. Figure 2(c) shows the corresponding power spectral density plot for the sample fatigue loading signals in Figure 2(a). The rms values are included with the superscript sign '$^{+}$' used to denote the inclusion of the effect of mean stress and '*' used to denote values without the effect of mean stress. Figure 3 shows more examples of stress histories with different and more extreme skewness and kurtosis values. Figure 3(a) shows the plot of the

stress history signals while 3(b) shows the histogram distribution of the data values. As in Figure 2(c), Figure 3(c) shows some of the underlining power spectral densities that were used to generate the signals in Figure 3(a). The full list of PSD types used can be found in reference [30] These plots and Table 2 show that a wide variety of materials, spectral properties, skewness and kurtosis values were covered in the work.

6.2 Trends of predictions using different types of ANN models.

This section shows the trends of predictions using different forms of ANN, i.e. *N1* to *N4* on 5 groups of signal types *T0* to *T4* comparing predictions with target values. The description of the signal types and ANN models are given in sections 2 and 4.2 respectively. Comparisons are also made with results of predictions using Dirlik[1] and Nieslony's[47] methods. Additionally, a comparison is also made with the use of the Benasciutti – Tovo method [29] together with the non Gaussian correction factor presented by Bracessi et al[41]. This correction factor is here given in equation (21). In applying this method, a Gaussian signal was first generated using equation (1) and then the corresponding non Gaussian signal was generated using the Winterstein leptokurtic equations (11) and (12). Signal type *T3* follows this approach and it is the signal choice made here for comparison. The non–Gaussian damage was then obtained using equation (21).

Figure 4 shows the plot of the trend of predictions for the signal type T0 using the ANN methods against target rainflow prediction. It also includes similar results for the Dirlik and Nieslony predictions. Each plot was based on 1000 generated signals. As can be seen in the plots in the figure all methods appear to produce good result. The coefficient of fit and the correlation coefficients all appear to be very good. The performance of Dirlik and Nieslony methods are also very good but this is not surprising because these were the type of signals used in the development of the methods.

Figure 5 shows the performance of all models on signal types *T1*, which have non zero, mean stress. Only the ANN models could be seen to give good correlation and fit. Similar trends can be seen for other signal types *T2* to *T4* are shown in Figures 6 to 8. It can be seen that the ANN models produced the best trends for all these non-Gaussian signals. The performance of the Dirlik and Nieslony methods for the type *T4* can be seen to be particularly wide. These methods although tempting to be used in all cases were not designed to be used for signals such as non-Gaussian distribution fatigue load. Figure 9 shows the plot of the results of using Benasciutti and Tovo [29] method together with Bracessi's [41] non Gaussian damage correction equation (21). It can be seen that the performance of the combination still does not match that of ANN. In some cases, the deviation can be quite significant perhaps because of the exponent factor involved in equation (22). Although all the ANN models performed well generally, it is helpful to try to identify which is best performing in most cases.

6.3 Performance of the ANN models

As highlighted in section 6.2 all the ANN models produced very good results. This section aims to look more closely at the predictions from all the models in order to identify which is best in most cases for all signal types. In order to achieve this aim, more extensive tests were carried out. Similar to section 6.2, 1000 signals were generated for an analysis. In this case, however, the analysis were repeated 10 times. For each test, the correlation coefficient and the coefficient of linear fit between the target and the predicted results were obtained for all the ANN models. The coefficient was obtained as the gradient of the line of best fit, $m = cov(X,Y)/var(X)$, where X and Y represent the rainflow calculated damage and the predicted damage $E(D)$ values respectively; *cov* and *var* are statistical symbols for covariance and variance respectively. This process was carried out twice which led to the results presented in the Tables 3 and 4. As can been in the results in the tables, all models were qualitatively very good. In some parts, the differences between the predictions are nominal and marginal. In order to obtain a quantitative

appraisal, the average of all RMS error and coefficient of fit and their corresponding standard deviations for all cases considered were determined. This showed that model N2 had the lowest error and model N4 had the best coefficient of fit. Model N2 had higher coefficient of fit of 0.975 and model N4 averaged to 0.999. The corresponding standard deviation on the coefficient of fit were 0.0361 and 0.0436 respectively. These results show that model N4 is likely to give results that will be closer to actual values than model N2 but the scatter in model N4 results is likely to be higher. These features can be seen in the trends shown in the plots in Figures 4 to 8. Better correspondence with actual results for model N4 makes it to be desirable compared to model N2.

Table 5 shows the comparison of the run times obtained using the tic toc commands recommended in MATLAB [44] for the comparison of the performance of algorithms. The run times were the times taking to process 10,000 signals to obtain the necessary input parameters and then using the ANN weights to make damage prediction as well as the times taken using the rainflow method to determine the range and mean stress values and using the material properties to obtain damage. The run times varied from 10.54 seconds for the N1 ANN type to 12.09 for the N4 type ANN. These performances compares with 40.11 seconds for the rainflow counting algorithm. This shows that the rainflow counting method required nearly 4 times as long time as the ANN methods.

6.4 Performance of ANN on random loading fatigue experimental test data.

The ANN model N4 herein was used to predict fatigue failure based on SAE experimental fatigue test data [48]. The data was generated in the early 1970s by the SAE in order to test the performance of different methods of calculating fatigue damage from random loading data. Two types of steel materials, Manten and RQC 100, were considered. Using one of the nominal fatigue stress analysis methods in [1]. The fatigue mechanical properties a and b based on

equation (17) which accounts for the effect of the stress concentration at the notch in the specimen are 2641 (MPa) and -0.248 for the Manten steel and 3336 (MPa) and -0.228 for the RQC 100 material respectively. Three forms of component loading were considered; these were representative of bracket, transmission and axle loading in a vehicle. Also, three load levels representing low, medium and high values were considered. The digitised versions of the loading forms could be found in finite element analysis packages such as ANSYS[49] and SolidWorks[50]. Figures 10 and 11 show the specimen geometry and the time history data for the SAE fatigue loading program respectively. As can be seen in the skewness and kurtosis values in Figure 10, the bracket data is platykurtic while the transmission and suspension data are mildly leptokurtic. Figure 12 shows the cumulative distribution counts for the stress range obtained from the loading data using the rainflow counting method[42]. The agreement between the plot in Figure 12 and that of the original plot by SAE in reference [42] was assuring that the data was right and that the in house routine used for the rainflow counting was correct.

The analysis to obtain the nominal stress in the net section can be carried out by modelling the test specimen as a simple beam subjected to both tension and bending loads as illustrated in Figure 10 [51]. This gives a value of 11.2 MPa/kN of the applied load. This implies that the nominal maximum stress σ_{max} for an applied load P in kN is 11.2 P (MPa). This value is then used together with the data points in Figure 10 to obtain the time domain series for any given load and for a specific component, i.e. bracket, transmission or suspension. The rainflow counting method can then be used to obtain a time domain damage value. The spectral moments were obtained as highlighted in section 3 and the procedures explained in sections 4 and 5 were used to obtain the ANN predictions for the fatigue damage.

The ANN results for damage obtained are plotted in Figures 12 and compared with those obtained based on time domain rainflow counting and of other frequency domain based

methods such as Dirlik[1] and Nieslony's[47] methods. As can be seen from the results, apart from the results for transmission, the ANN predictions are generally closer to experimental results than those of any previous frequency domain based methods. It is surprising that although the rainflow counting method gives closer results to experimental values in magnitude the trend in terms of over predicting or under predicting cannot be assumed. This makes the use of other methods such as the ANN to be helpful in obtaining as much information as possible for the design of effective components for life application. It should also be remarked that the ANN model which includes skewness and kurtosis effects still predict good results without noticeable reduction in performance compared to previous ANN models that used less number of inputs[30, 31, 43].

7. Discussion

The results in this work have shown ANN to be a versatile approach in developing predictive models that can have many input parameters. As highlighted in the results section, it has been encouraging to identify the output required for ANN to be able to predict with good degree of correlation and fit the results for both Gaussian and non-Gaussian fatigue problems. The ANN model N4 gave better fit to target results generally for all types of fatigue data form than the lower order ANN models that require less input parameters. The prediction of the model however, appear to exhibit nominally higher scatter in results than lower order methods. This may be partly due to the higher order spectral variables m_5 and m_6 that are included in its input. These are based on products of the fifth and sixth order with respect to frequency. This higher order can lead to amplification of differences. Model *N4* should be generally preferable than others because it is not always the case that the form of loading of a fatigue data is known in advance. An encompassing model such as N4 is more likely to capture the prediction generally better than using a lower-order model for a higher order complex data. The results in this work also show again as in reference [31] that existing frequency domain methods are not capable of handling the effect of mean stress on fatigue damage effectively. It should also be reiterated

that the results of the rainflow counting time-domain method is not necessary always consistent in over predicting or under predicting fatigue damage.

8. Conclusion

An ANN model that is capable of predicting fatigue damage under Gaussian and non Gaussian load distribution has been presented. A wide range of skewness and kurtosis values were considered. Both platykurtic and leptokurtic distribution data types were considered. The prediction of the ANN model is very good compared to target values and better than those of other frequency domain methods. The ANN method was validated against experimental results produced by the SAE for random fatigue loading analysis demonstrating the viability of the method. The results ofthe ANN methods for fatigue damage values were generally between those of other spectral methods and that of the rainflow counting time domain method. For the cases considered, the ANN approach generates damage predictions about four times faster than the rainflow counting method.

List of Tables

Table 1 Input and output variables defining the ANN models N1 to N4

Table 2 Limits of property and spectral moments considered

Table 3 RMS error and coefficient of fit for results of various trials using ANN models N1 to N4 – Test 1

Table 4 RMS error and coefficient of fit for results of various trials using ANN models N1 to N4 – Test 2

Table 5 Performance indicators using tic toc run time in MATLAB for different ANN network types and rainflow counting method. Number of signals analysed in each run was 10,000.

List of Figures

Figure 1 ANN architecture

Figure 2(a) Sample fatigue loading signals with different skewness and kurtosis values

Figure 2(b) Corresponding histogram for the sample fatigue loading signals in Figure 2(a)

Figure 2(c) Corresponding PSD plots for the sample fatigue loading signals in Figure 2(a)

Figure 3(a) Sample fatigue loading signals including extreme skewness and kurtosis values

Figure 3(b) Corresponding histogram for the sample fatigue loading signals in Figure 3(a)

Figure 3(c) Corresponding PSD plots for the sample fatigue loading signals in Figure 3(a)

Figure 4 Trends of predictions of ANN models N1 to N4 with target values and Dirlik[1] and Nieslony[47] methods for signal type T0

Figure 5 Trends of predictions of ANN models N1 to N4 with target values and Dirlik and Nieslony methods for signal type T1

Figure 6 Trends of predictions of ANN models N1 to N4 with target values and Dirlik and Nieslony methods for signal type T2

Figure 7 Trends of predictions of ANN models N1 to N4 with target values and Dirlik and Nieslony methods for signal type T3

Figure 8 Trends of predictions of ANN models N1 to N4 with target values and Dirlik and Nieslony methods for signal type T4

Figure 9 Trends of predictions of ANN models N1 to N4 with target values and Nieslony and Benasciutti – Tovo methods for signal type T3

Figure 10 Illustration of SAE fatigue specimen, L = 60.84 mm, W = 66.13 mm, Thickness = 9.5 mm

Figure 11 Stress histories developed by SAE [48] for the random loading fatigue experiment (a) Bracket, (b) Transmission, (c) Suspension.

Figure 12 Distribution of stress range values obtained using rainflow counting for the SAE [48] random loading fatigue experiment (a) Bracket, (b) Transmission, (c) Suspension assuming maximum stress value of 1000 MPa for the signal

Figure 13 (a) Manten fatigue life results from A – Experiment, B – Rainflow, C – ANN N4, D – Dirlik [1], E – Nieslony's method [47]

Figure 13 (b) RQC-100 fatigue life results from A – Experiment, B – Rainflow, C – ANN, D – Dirlik [1], E – Nieslony's method [47]

References

1. Dirlik, T., *Application of computers in fatigue analysis*. 1985, University of Warwick.
2. Petrucci, G., M. Di Paola, and B. Zuccarello, *On the characterization of dynamic properties of random processes by spectral parameters.* Journal of applied mechanics, 2000. **67**(3): p. 519-526.
3. Kihl, D.P., S. Sarkani, and J.E. Beach, *STOCHASTIC FATIGUE DAMAGE ACCUMULATION UNDER BROAD-BAND LOADINGS.* International Journal of Fatigue, 1995. **17**(5): p. 321-329.
4. Rice, S.O., *Mathematical analysis of random noise.* Bell System Technical Journal, 1944. **23**(3): p. 282-332.
5. Mršnik, M., J. Slavič, and M. Boltežar, *Frequency-domain methods for a vibration-fatigue-life estimation–Application to real data.* International journal of fatigue, 2013. **47**: p. 8-17.
6. Kihm, F., N.S. Ferguson, and J. Antoni, *Fatigue life from kurtosis controlled excitations.* Procedia Engineering, 2015. **133**: p. 698-713.
7. Smallwood, D.O., *Generating non-Gaussian vibration for testing purposes.* Sound and Vibration, 2005. **39**(10): p. 18-23.
8. Wolfsteiner, P. and W. Breuer, *Fatigue assessment of vibrating rail vehicle bogie components under non-Gaussian random excitations using power spectral densities.* Journal of Sound and Vibration, 2013. **332**(22): p. 5867-5882.
9. Huang, G., et al., *Uncertainty of peak value of non-Gaussian wind load effect: Analytical approach.* Journal of Engineering Mechanics, 2017. **144**(2): p. 04017172.
10. Kihm, F., et al., *Understanding how kurtosis is transferred from input acceleration to stress response and it's influence on fatigue life.* 2013.
11. Wolfsteiner, P. and A. Trapp, *Fatigue life due to non-Gaussian excitation-an analysis of the Fatigue Damage Spectrum using Higher Order Spectra.* International Journal of Fatigue, 2019.
12. Nichols, J., et al., *A simple algorithm for generating spectrally colored, non-Gaussian signals.* Probabilistic Engineering Mechanics, 2010. **25**(3): p. 315-322.
13. Rouillard, V. *On the Non-Gaussian Nature of Random Vehicle Vibrations*. in *World Congress on Engineering*. 2007.
14. Winterstein, S.R., *Nonlinear vibration models for extremes and fatigue*. Journal of Engineering Mechanics, 1988. **114**(10): p. 1772-1790.
15. Sobczyk, K. and B. Spencer Jr, *Random fatigue: from data to theory*. 2012: Academic Press.
16. Lalanne, C., *Mechanical Vibration and Shock Analysis, Random Vibration*. Vol. 3. 2014: John Wiley & Sons.
17. Wikipedia. *Beta distribution*. [cited 2019 24th April]; Available from: https://en.wikipedia.org/wiki/Beta_distribution.

18. Cianetti, F., et al., *Correction formula approach to evaluate fatigue damage induced by non-Gaussian stress state.* Procedia Structural Integrity, 2018. **8**: p. 390-398.
19. Niesłony, A., et al., *The use of spectral method for fatigue life assessment for non-gaussian random loads.* acta mechanica et automatica, 2016. **10**(2): p. 100-103.
20. BöhM, M. and T. Łagoda, *Fatigue life assessment with the use of the spectral method for non-Gaussian loading histories with the use of the energy parameter.* Journal of Machine Construction and Maintenance. Problemy Eksploatacji, 2018.
21. Benasciutti, D. and R. Tovo, *Cycle distribution and fatigue damage assessment in broad-band non-Gaussian random processes.* Probabilistic Engineering Mechanics, 2005. **20**(2): p. 115-127.
22. HKDH, B., *Neural networks in materials science.* ISIJ international, 1999. **39**(10): p. 966-979.
23. Artymiak, P., et al., *Determination of S–N curves with the application of artificial neural networks.* Fatigue & Fracture of Engineering Materials & Structures, 1999. **22**(8): p. 723-728.
24. Pujol, J.C.F. and J.M.A. Pinto, *A neural network approach to fatigue life prediction.* International Journal of Fatigue, 2011. **33**(3): p. 313-322.
25. Iacoviello, F., D. Iacoviello, and M. Cavallini, *Analysis of stress ratio effects on fatigue propagation in a sintered duplex steel by experimentation and artificial neural network approaches.* International Journal of Fatigue, 2004. **26**(8): p. 819-828.
26. Kim, Y., H. Kim, and I.-G. Ahn, *A study on the fatigue damage model for Gaussian wideband process of two peaks by an artificial neural network.* Ocean Engineering, 2016. **111**: p. 310-322.
27. Wirsching, P.H. and M.C. Light, *Fatigue under wide band random stresses.* Journal of the Structural Division, 1980. **106**(7): p. 1593-1607.
28. Zhao, W. and M.J. Baker, *On the probability density function of rainflow stress range for stationary Gaussian processes.* International Journal of Fatigue, 1992. **14**(2): p. 121-135.
29. Benasciutti, D. and R. Tovo, *Spectral methods for lifetime prediction under wide-band stationary random processes.* International Journal of Fatigue, 2005. **27**(8): p. 867-877.
30. Durodola, J., et al., *A pattern recognition artificial neural network method for random fatigue loading life prediction.* International Journal of Fatigue, 2017. **99**: p. 55-67.
31. Durodola, J.F., et al., *Artificial neural network for random fatigue loading analysis including the effect of mean stress.* International Journal of Fatigue, 2018. **111**: p. 321-332.
32. Bishop, C.M., *Neural networks for pattern recognition*. 1995: Oxford university press.
33. Farley, S.J., et al., *High resolution non-destructive evaluation of defects using artificial neural networks and wavelets.* Ndt & E International, 2012. **52**: p. 69-75.
34. Farley, S.J., et al., *A Neural Network Approach for Locating Multiple Defects*, in *Advances in Experimental Mechanics Vi*, J.M. DulieuBarton, J.D. Lord, and R.J. Greene, Editors. 2008. p. 125-131.
35. Hernandez-Gomez, L.H., et al., *Locating defects using dynamic strain analysis and artificial neural networks*, in *Advances in Experimental Mechanics IV*, J.M. DulieuBarton and S. Quinn, Editors. 2005. p. 325-330.
36. Luna-Aviles, A., et al., *Locating and Classifying Defects with Artificial Neural Networks*, in *Advances in Experimental Mechanics Vi*, J.M. DulieuBarton, J.D. Lord, and R.J. Greene, Editors. 2008. p. 117-123.
37. Shinozuka, M., *Monte Carlo solution of structural dynamics.* Computers & Structures, 1972. **2**(5-6): p. 855-874.
38. NIST/SEMATECH. *Beta Distribution, e-Handbook of Statistical Methods*. 2012; Available from: https://www.itl.nist.gov/div898/handbook/eda/section3/eda366h.htm.

39. Quigley, J.P., Y.-L. Lee, and L. Wang, *Review and Assessment of Frequency-Based Fatigue Damage Models*. SAE International Journal of Materials and Manufacturing, 2016. **9**(2016-01-0369).
40. Dowling, N.E., *Mechanical behavior of materials: engineering methods for deformation, fracture, and fatigue*. 2012: Pearson.
41. Braccesi, C., et al., *The frequency domain approach in virtual fatigue estimation of non-linear systems: The problem of non-Gaussian states of stress.* International Journal of Fatigue, 2009. **31**(4): p. 766-775.
42. ASTM, E., *1049-85, "Standard practices for cycle counting in fatigue analysis".* Annual book of ASTM standards, 2005. **3**(01): p. 614-620.
43. Ramachandra, S., et al., *Experimental validation of an ANN model for random loading fatigue analysis.* International Journal of Fatigue, 2019. **126**: p. 112-121.
44. The MathWorks Inc(2018), *MATLAB The language of technical computing*. 2018: USA.
45. Mckay, M., R. Beckman, and W. Conover, *A Comparison of Three Methods for Selecting Values of Input Variables in the Analysis of Output from a Computer Code.* Technometrics, 2000: p. 55-61.
46. Montgomery, D.C., *Design and analysis of experiments*. 2008: John Wiley & Sons.
47. Niesłony, A. and M. Böhm, *Mean stress effect correction using constant stress ratio S–N curves.* International journal of fatigue, 2013. **52**: p. 49-56.
48. Bussa, S. and L. Tucker, *The SAE cumulative fatigue damage test program.* Paper, 1975. **750038**.
49. ANSYS, *ANSYS WORKBENCH.* ANASYS USA, 2018.
50. System, D., *SolidWorks* 2018
51. eFatigue, A. *SAE keyhole specimen*. 2019; Available from: https://www.efatigue.com/benchmarks/SAE_keyhole/SAE_keyhole.html.

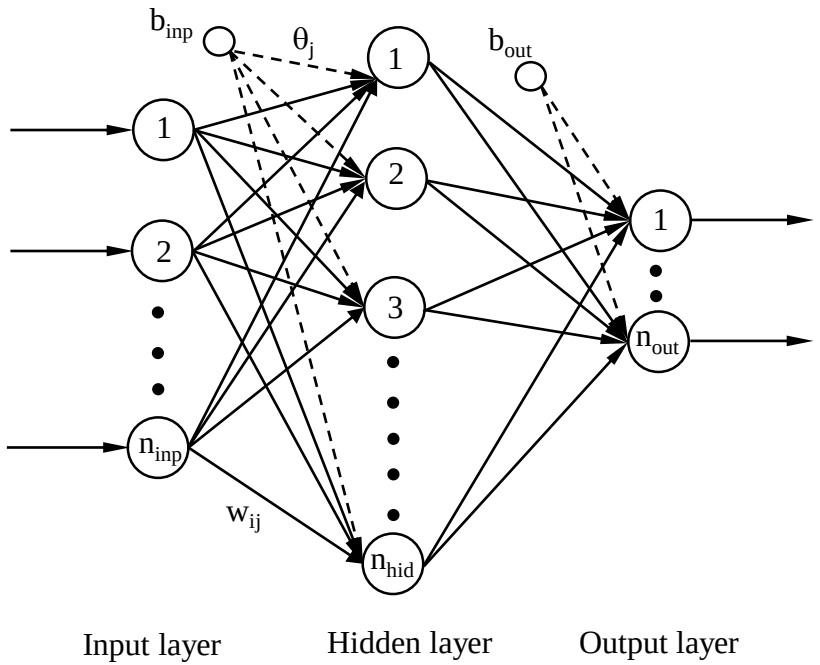

Figure 1 ANN architecture

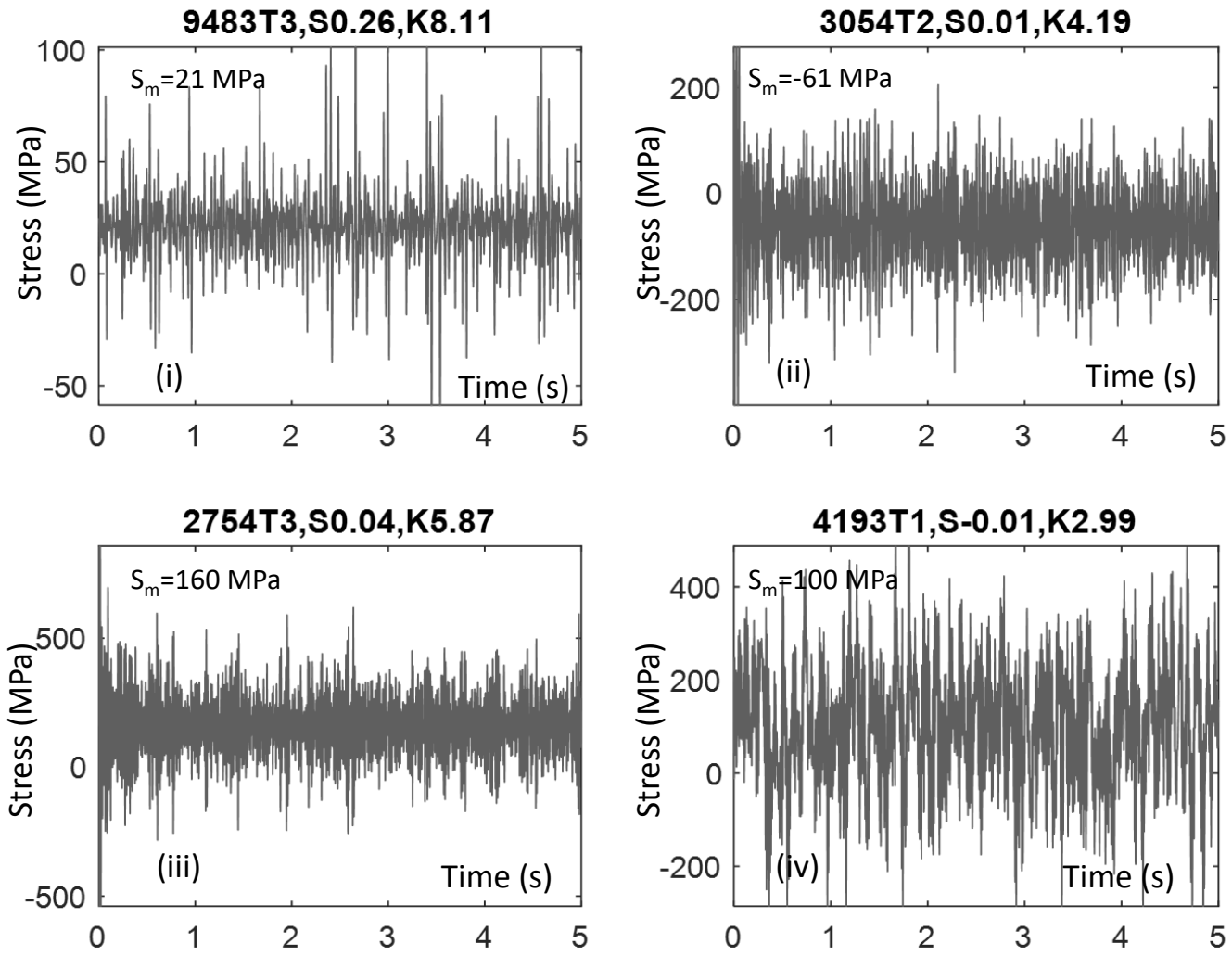

Figure 2(a) Sample fatigue loading signals with different skewness and kurtosis values

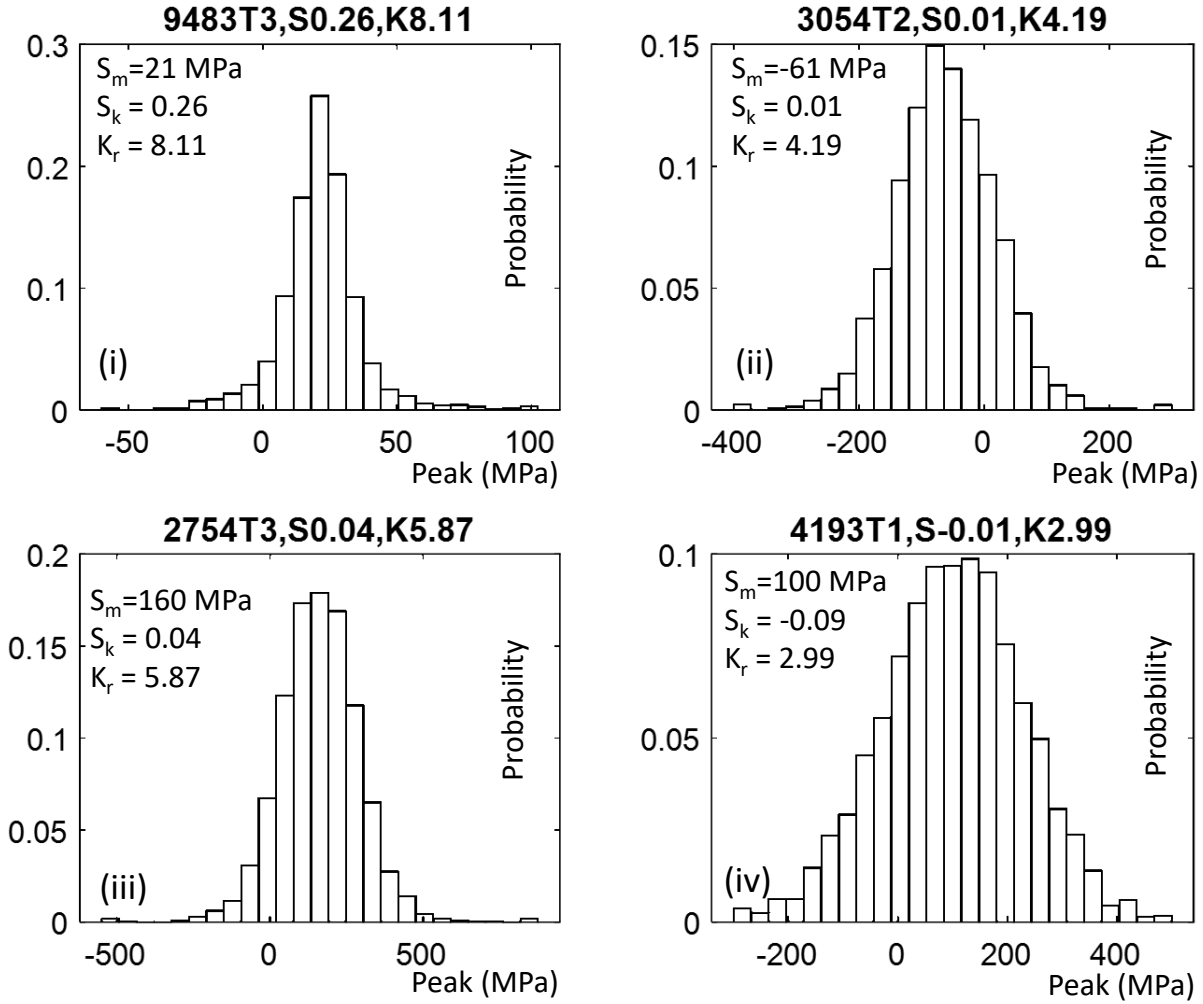

Figure 2(b) Corresponding histogram for the sample fatigue loading signals in Figure 2(a)

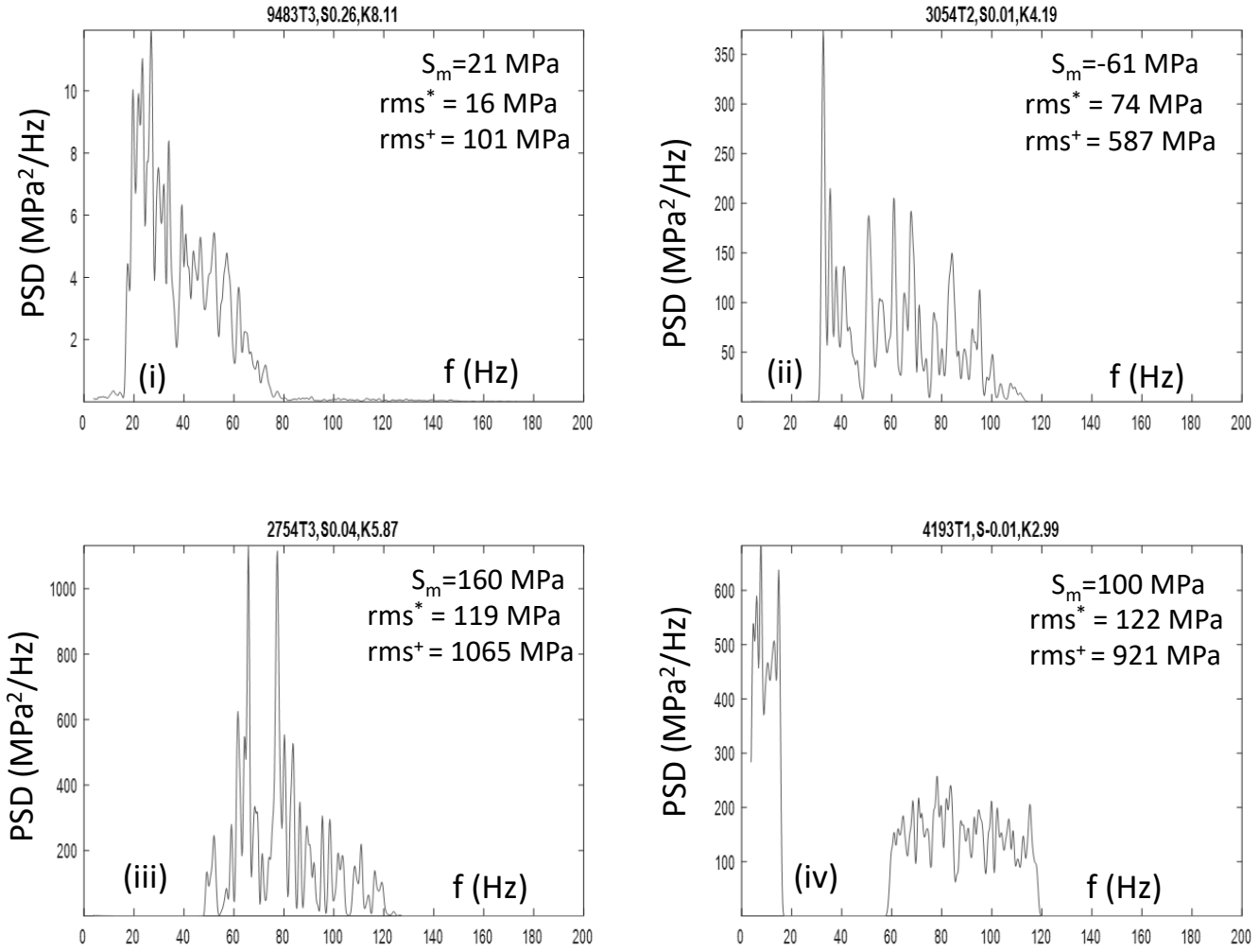

Figure 2(c) Corresponding power spectral density plot for the sample fatigue loading signals in Figure 2(a). The rms values are included with $^+$ used to denote the inclusion of the effect of mean stress and * used to denote values without the effect of mean stress

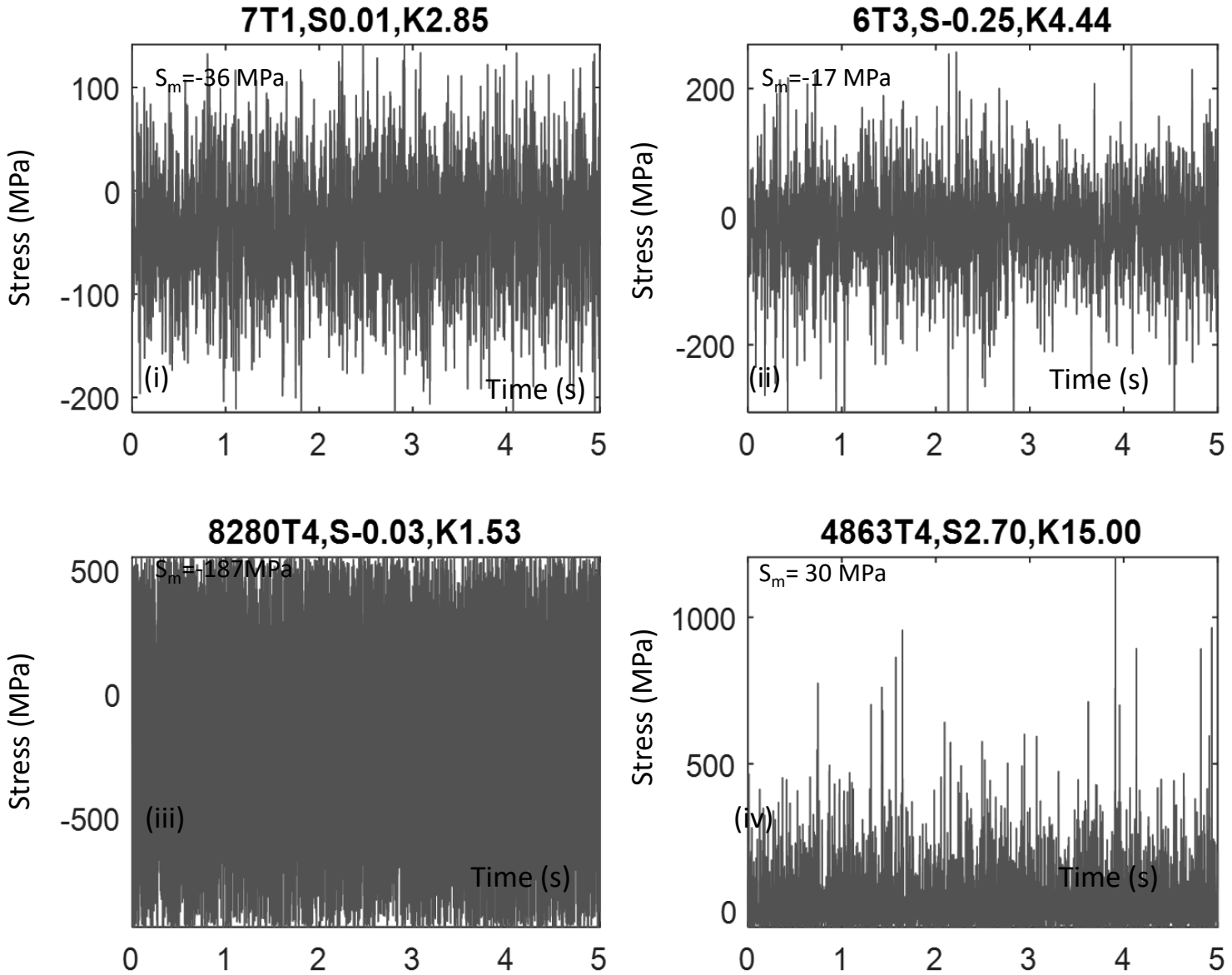

Figure 3(a) Sample fatigue loading signals including extreme skewness and kurtosis values

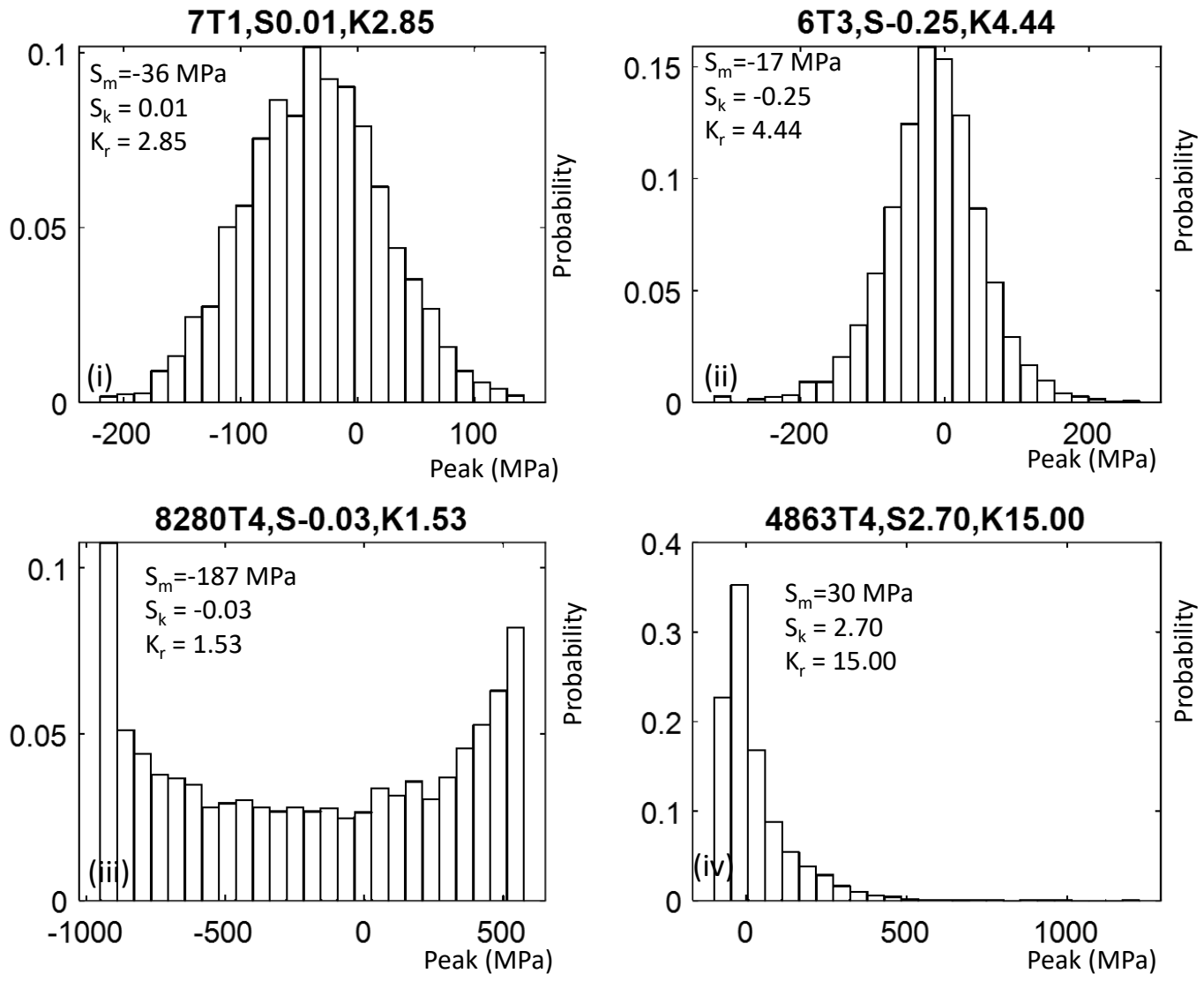

Figure 3(b) Corresponding histogram for the sample fatigue loading signals in Figure 3(a)

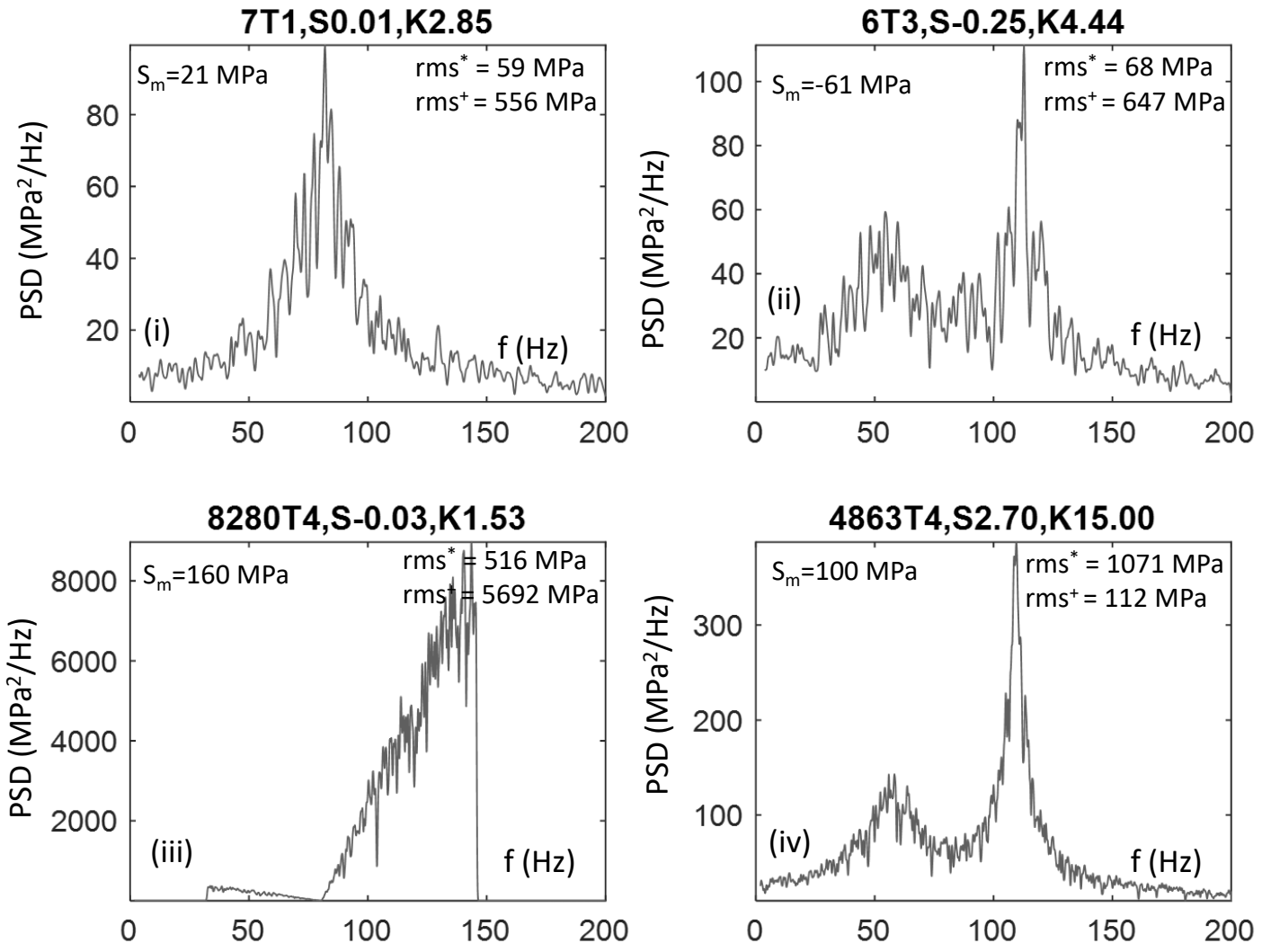

Figure 3(c) Corresponding power spectral density plot for the sample fatigue loading signals in Figure 3(a). The rms values are included with $^{+}$ used to denote the inclusion of the effect of mean stress and * used to denote values without the effect of mean stress

Type T0

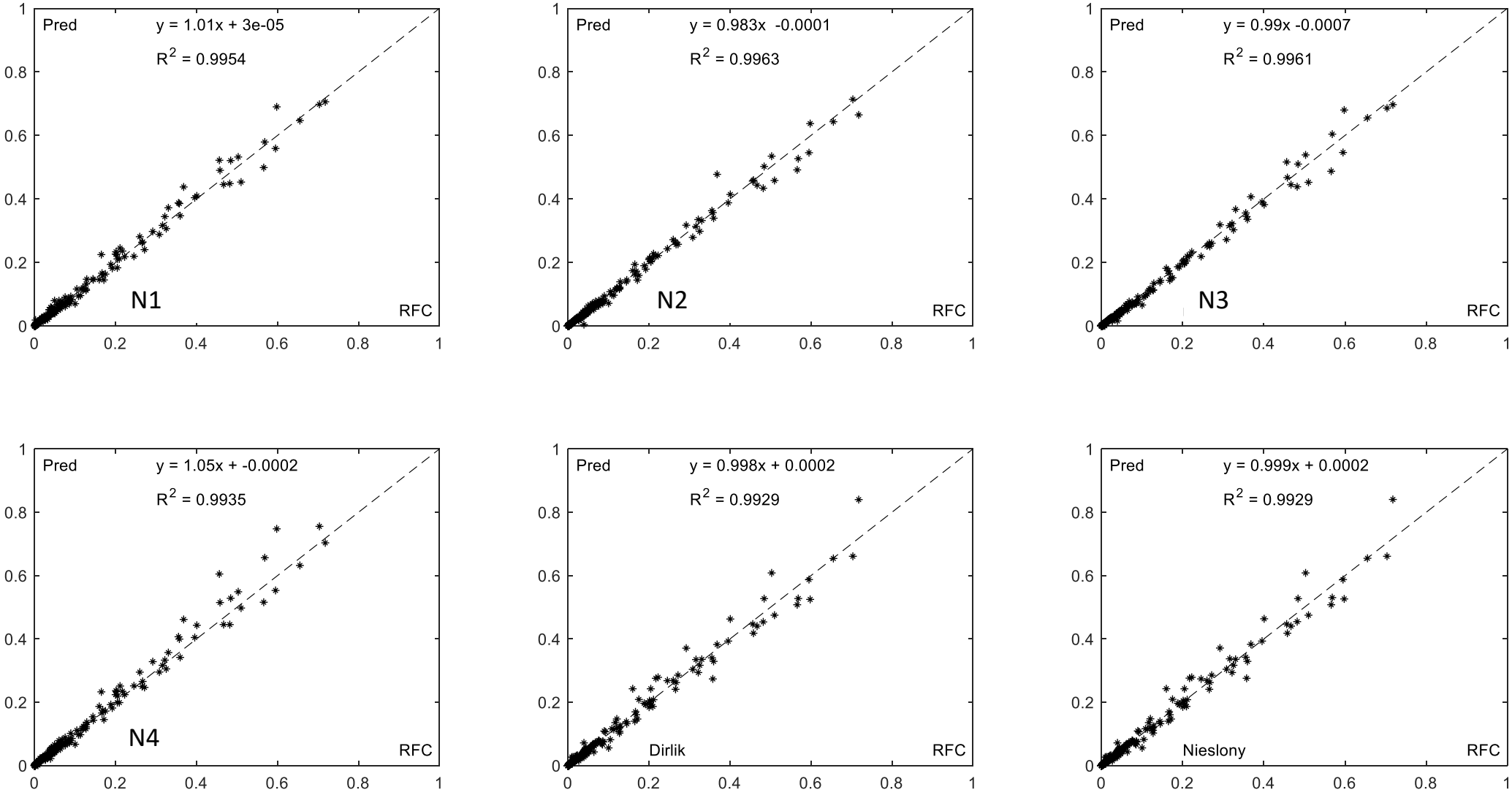

Figure 4 Trends of predictions of ANN models N1 to N4 with target values and Dirlik[1] and Nieslony[47] methods for signal type T0

Type T1

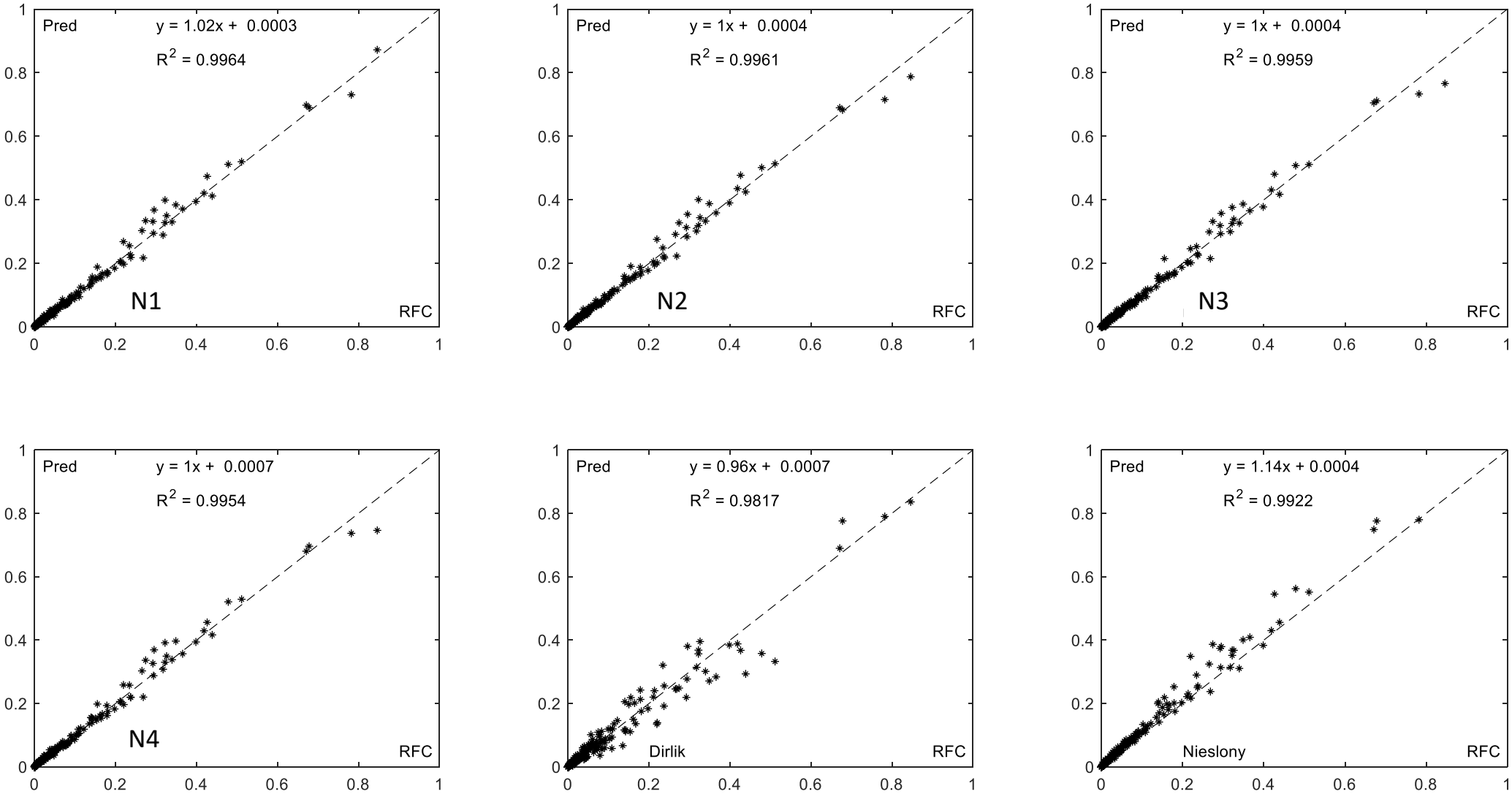

Figure 5 Trends of predictions of ANN models N1 to N4 with target values and Dirlik[1] and Nieslony[47] methods for signal type T1

Type T2

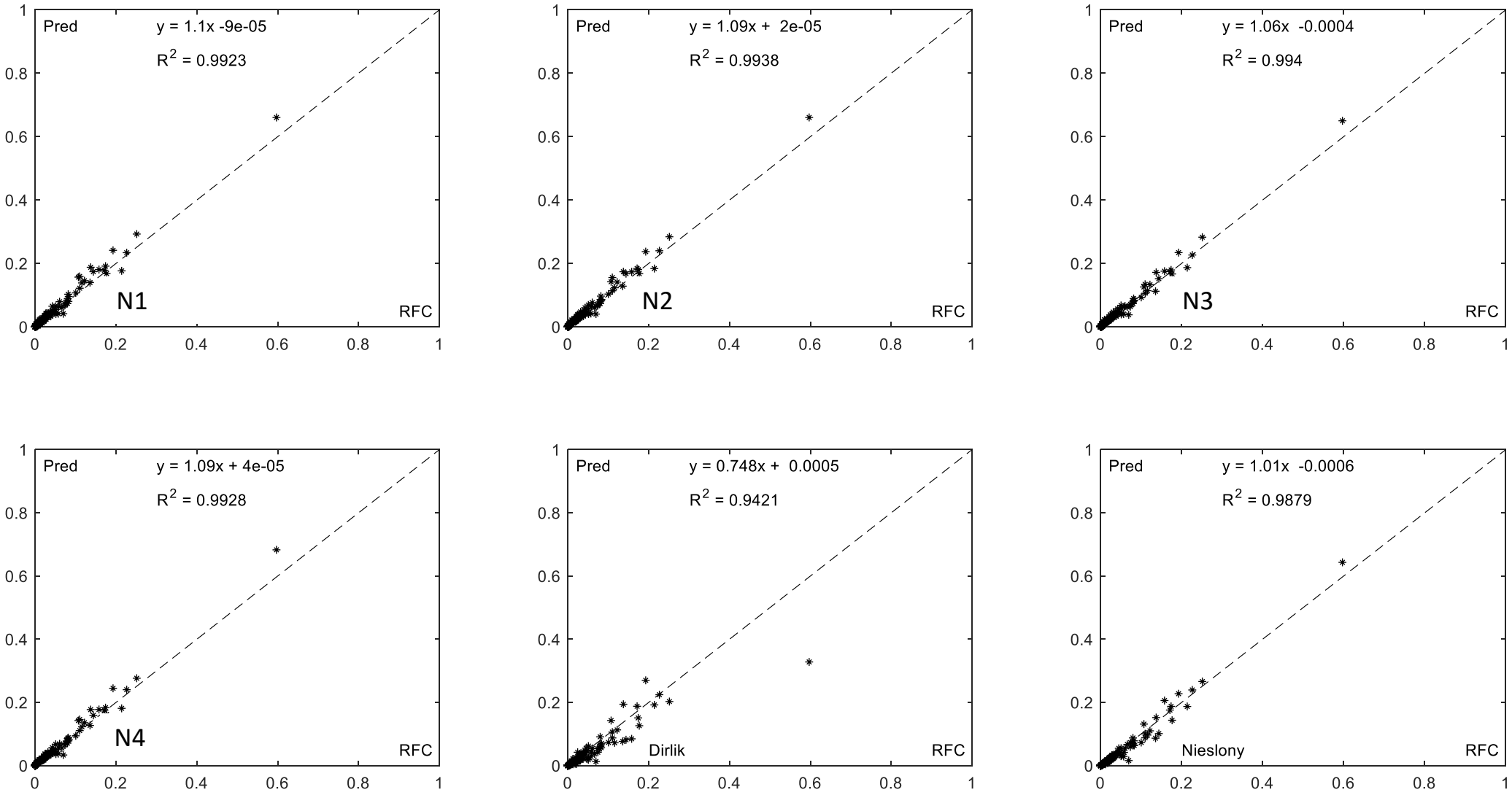

Figure 6 Trends of predictions of ANN models N1 to N4 with target values and Dirlik[1] and Nieslony[47] methods for signal type T2

Type T3

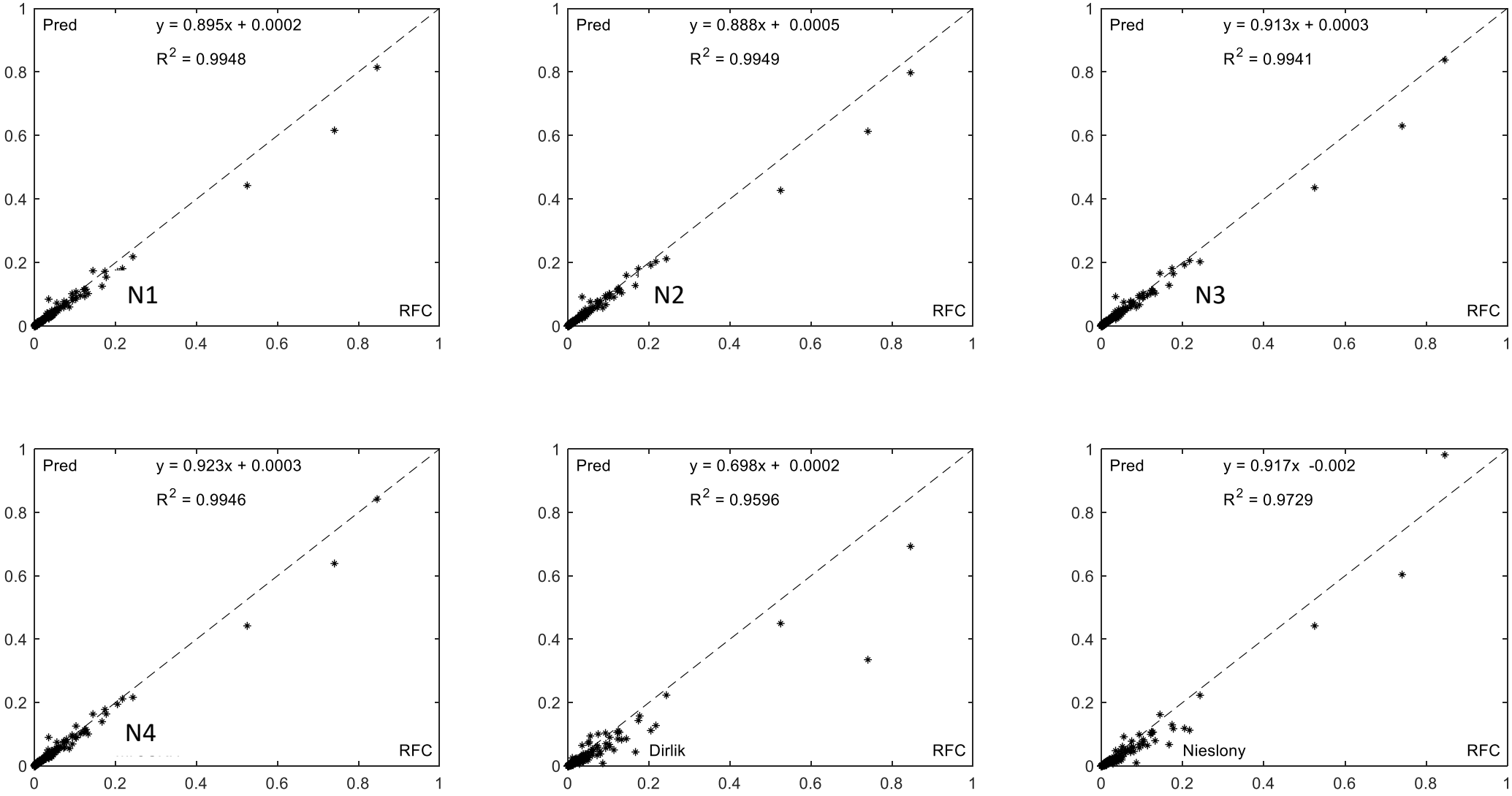

Figure 7 Trends of predictions of ANN models N1 to N4 with target values and Dirlik[1] and Nieslony[41] methods for signal type T3

Type T4

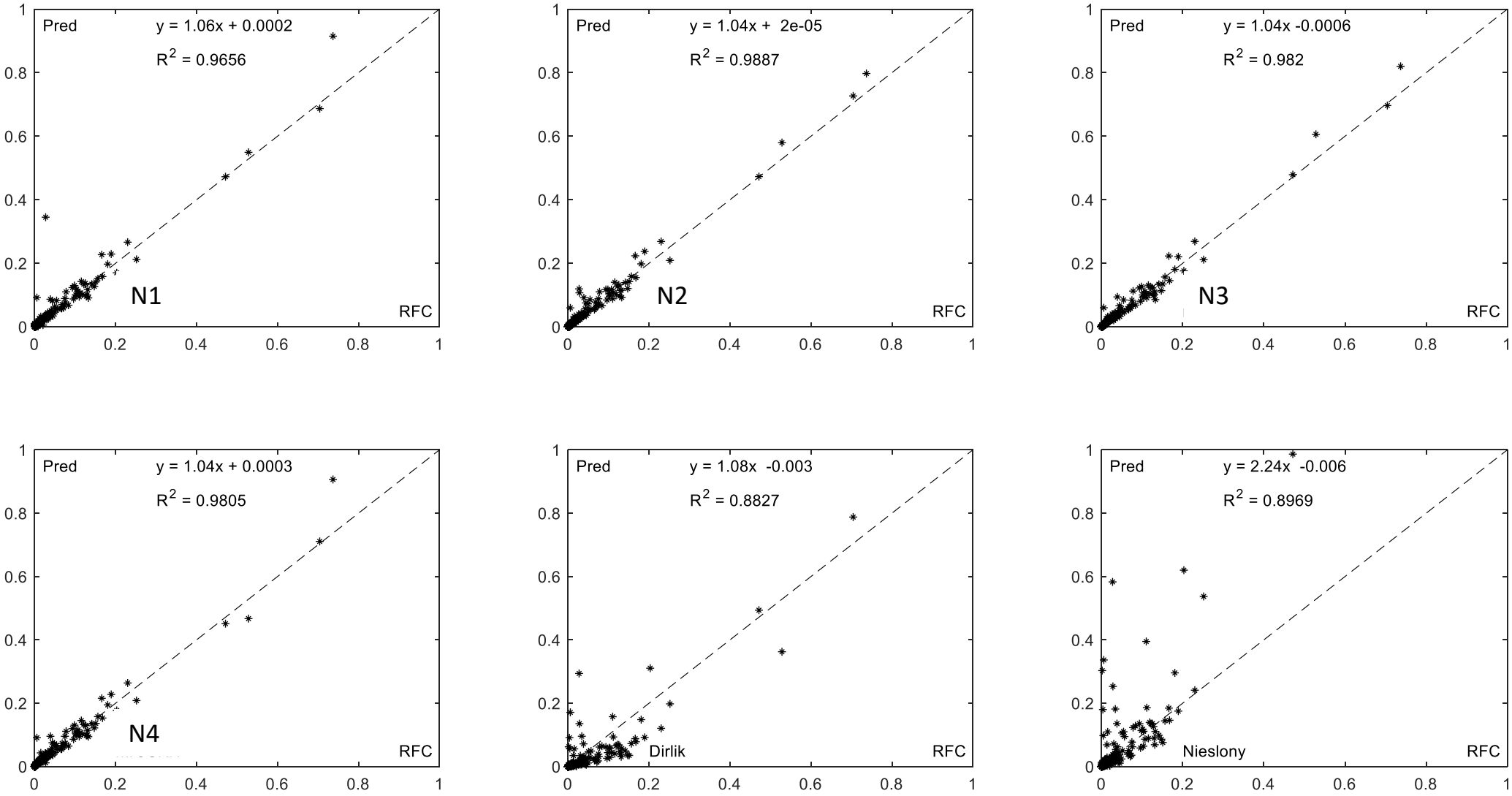

Figure 8 Trends of predictions of ANN models N1 to N4 with target values and Dirlik[1] and Nieslony[47] methods for signal type T4

Type T3 additional

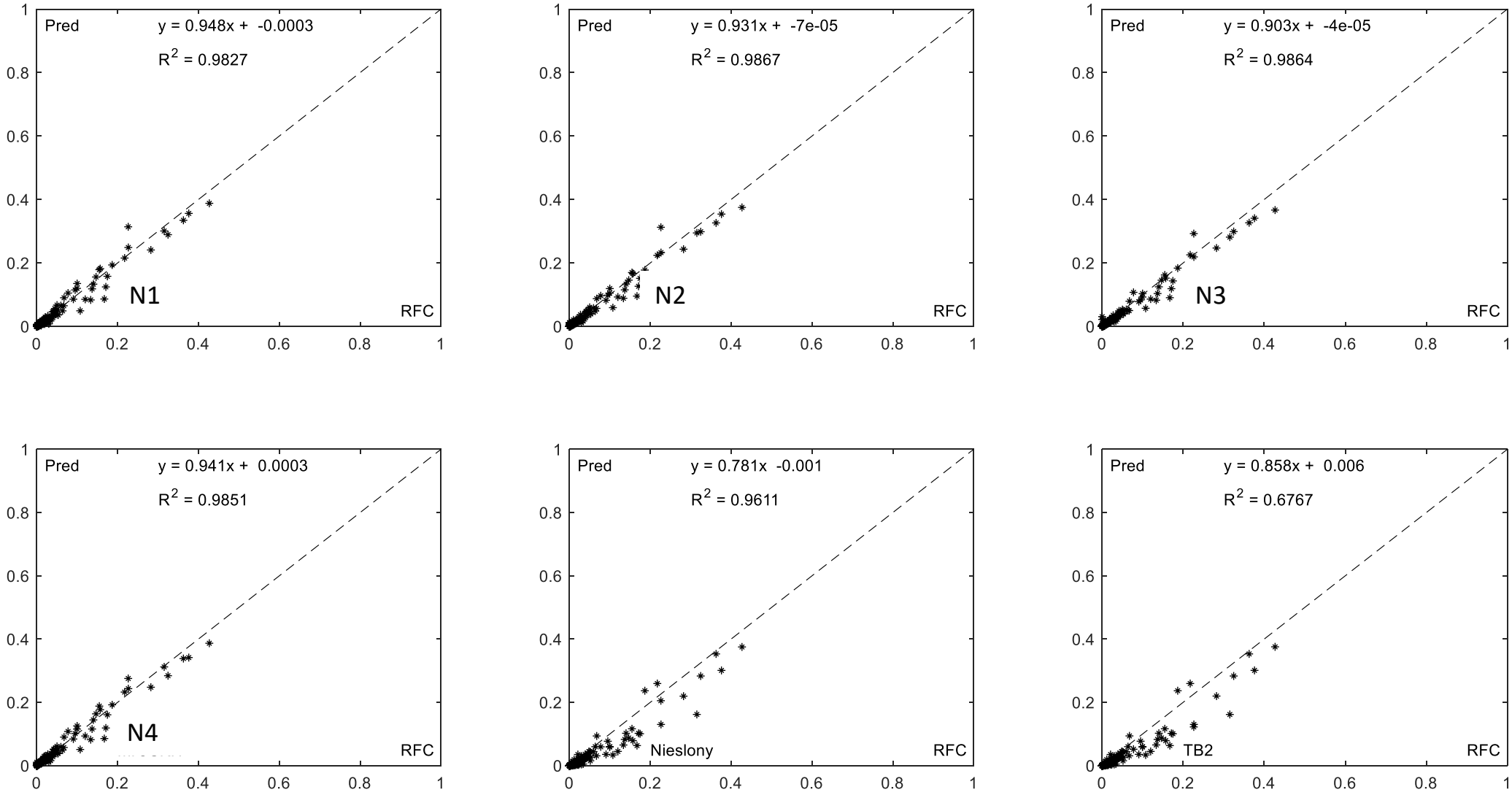

Figure 9 Trends of predictions of ANN models N1 to N4 with target values and Nieslony[19] and Benasciutti-Tovo [29] with Bracessi [41] non Gaussian fatigue damage correction factor methods for signal type T3

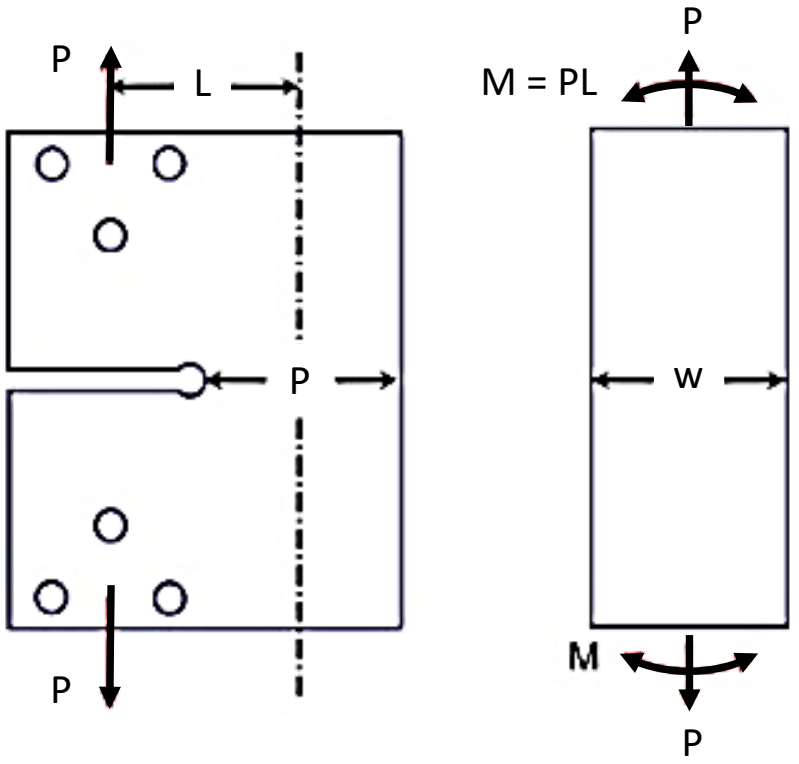

Figure 10 Illustration of SAE fatigue specimen [42,45], L = 60.84 mm, W = 66.13 mm, Thickness = 9.5 mm

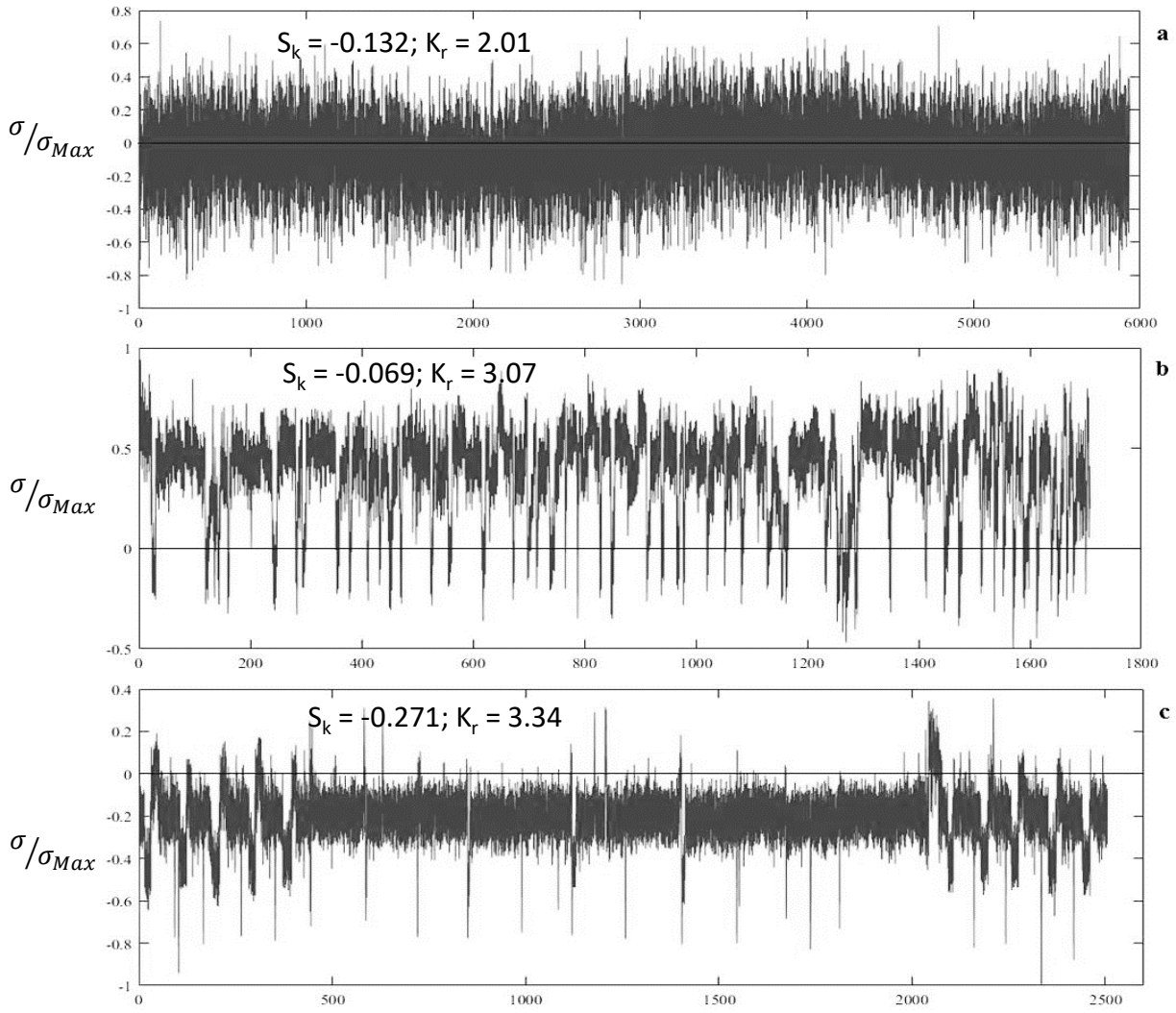

Figure 11 Stress histories developed by SAE [42] for the random loading fatigue experiment (a) Bracket, (b) Transmission, (c) Suspension.

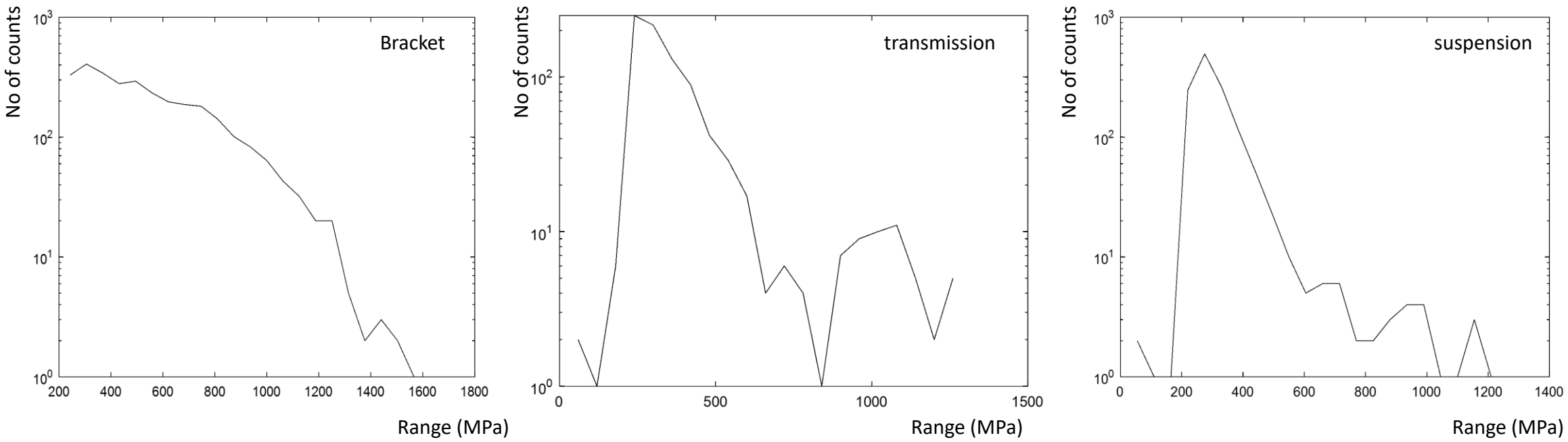

Figure 12 Distribution of stress range values obtained using rainflow counting for the SAE [42] random loading fatigue experiment (a) Bracket, (b) Transmission, (c) Suspension assuming maximum stress value of 1000 MPa for the signal

SAE Data

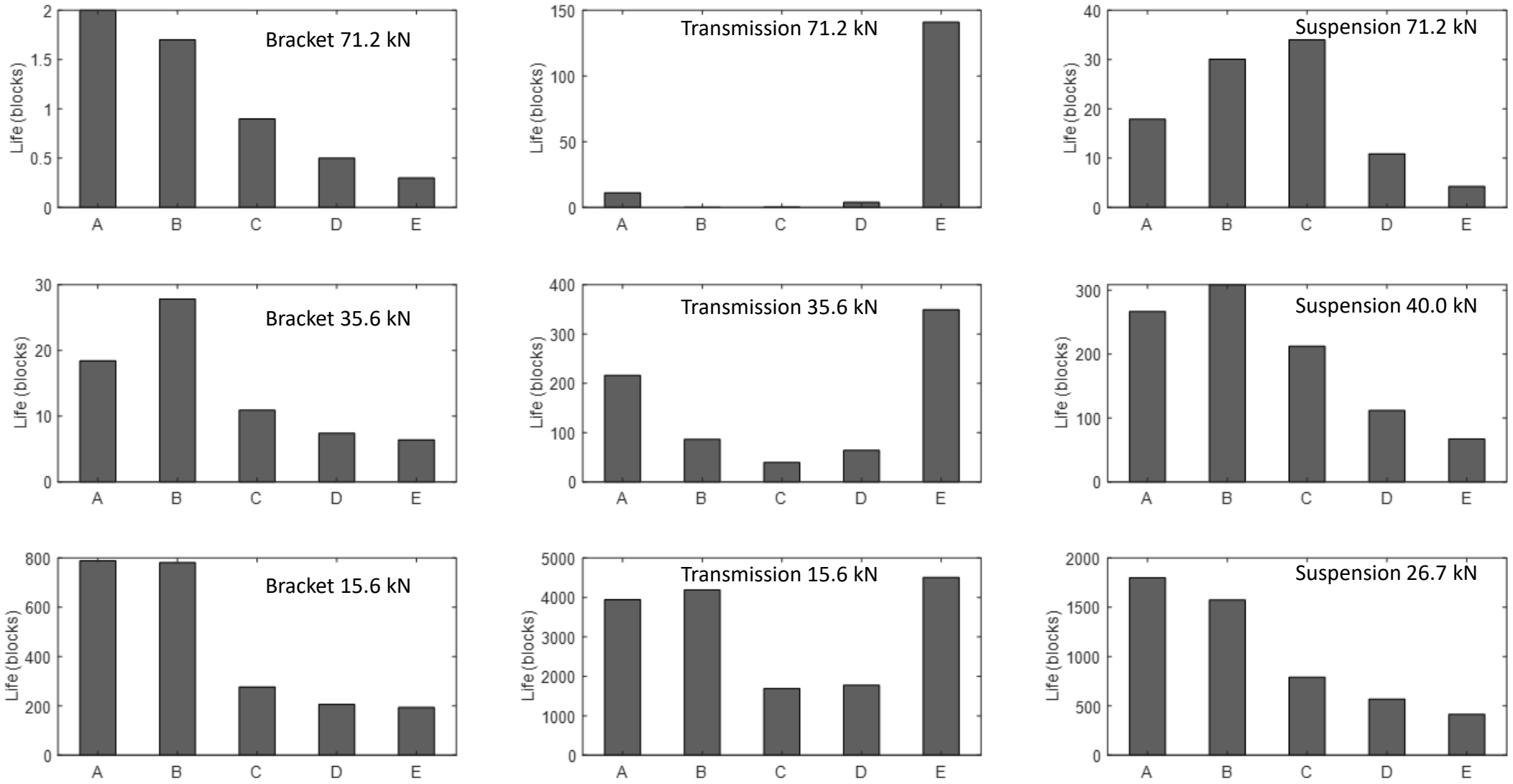

Figure 13 (a) Manten fatigue life results from A – Experiment, B – Rainflow, C – ANN N4, D – Dirlik[1], E – Nieslony's method[41]

SAE Data

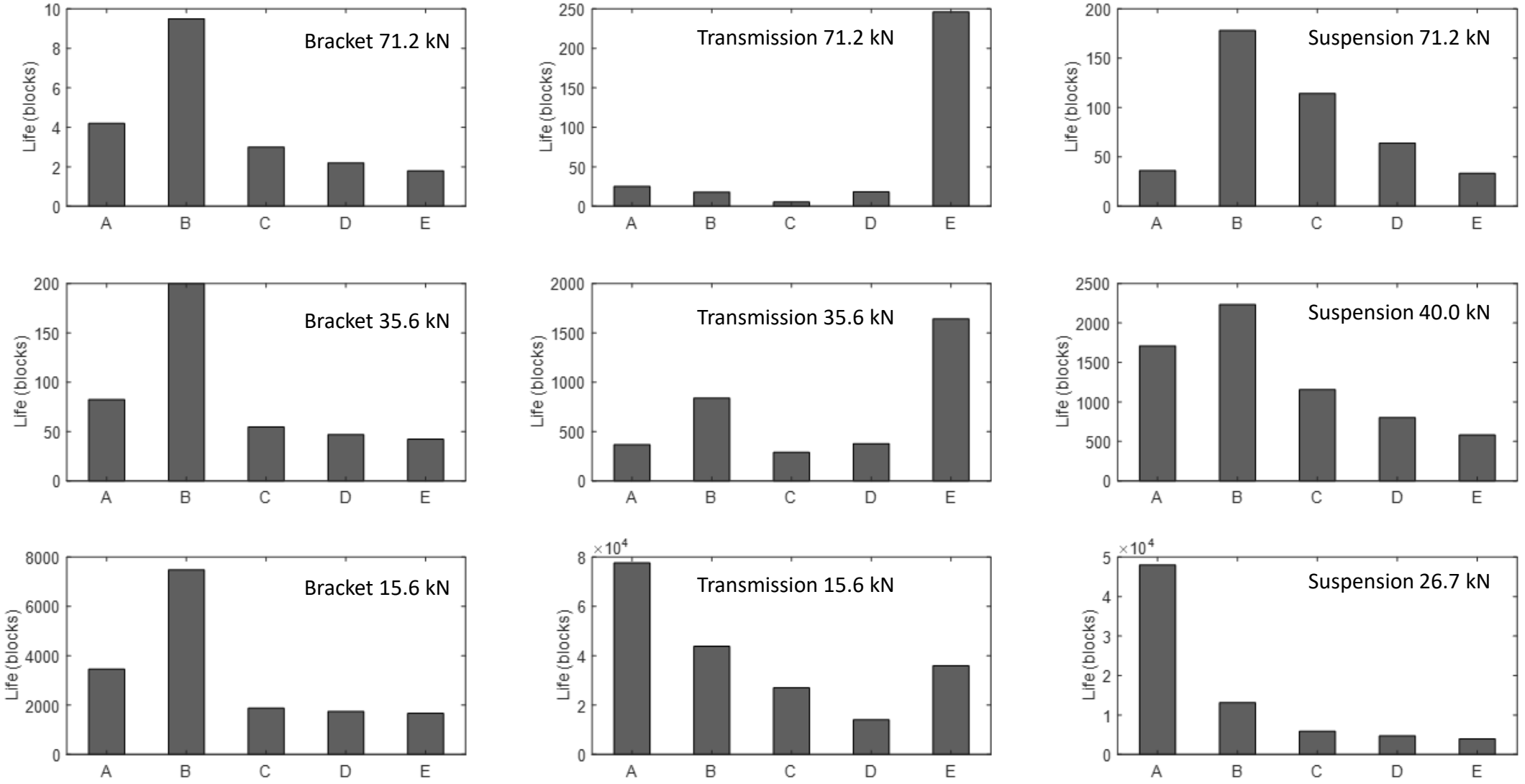

Figure 13 (b) RQC-100 fatigue life results from A – Experiment, B – Rainflow, C – ANN, D – Dirlik[1], E – Nieslony's method[47]

ANN type	No of inputs	Input	output
N1	*11*	$m_0, m_1, m_2, m_4, a, b, S_u, \alpha_m, \alpha_c, \gamma_p, \gamma_n$	$Log[E(D)]$
N2	*13*	$m_0, m_1, m_2, m_4, a, b, S_u, \alpha_m, \alpha_c, \gamma_p, \gamma_n, S, K$	
N3	*14*	$m_0, m_1, m_2, m_3, m_4, a, b, S_u, \alpha_m, \alpha_c, \gamma_p, \gamma_n, S, K$	
N4	*16*	$m_0, m_1, m_2, m_3, m_4, m_5, m_6\ a, b, S_u, \alpha_m, \alpha_c, \gamma_p, \gamma_n, S, K$	

Table 1 Input and output variables defining the ANN models *N1* to *N4*

Prop	S_u (MPa)	a (MPa)	b	m_0	m_1	m_2	m_3	m_4	m_5	m_6	S_k	K_r
Min	200	261	-0.333	4.74E+00	1.34E+02	3.33E+03	5.26E+04	5.07E+06	7.39E+08	1.22E+11	-0.69	1.55
Max	2000	26543	-0.085	1.23E+06	1.19E+08	1.19E+10	1.56E+12	2.19E+14	3.08E+16	4.33E+18	2.67	15.51

Table 2 Range of limits of fatigue parameters and spectral moments used in the study

Trials	RMS error				Coeff of fit			
	N1	N2	N3	N4	N1	N2	N3	N4
1	6.05E-05	5.25E-05	4.82E-05	8.69E-05	1.0283	1.0190	1.0243	1.0382
2	8.85E-05	7.22E-05	6.50E-05	1.45E-04	1.0343	1.0319	1.0197	1.0614
3	6.60E-05	5.44E-05	5.49E-05	1.09E-04	1.0218	1.0121	1.0172	1.0410
4	6.04E-05	4.86E-05	6.19E-05	7.12E-05	0.9959	1.0036	0.9895	1.0008
5	4.99E-05	4.69E-05	3.38E-05	4.92E-05	0.9990	0.9950	1.0001	1.0128
6	5.44E-05	4.37E-05	4.32E-05	5.43E-05	1.0229	1.0162	1.0220	1.0408
7	4.74E-05	7.49E-05	5.86E-05	1.07E-04	1.0136	0.9811	1.0053	1.0438
8	7.59E-05	6.37E-05	7.73E-05	6.95E-05	0.9889	0.9780	0.9951	1.0215
9	3.40E-05	2.88E-05	2.82E-05	6.48E-05	1.0130	1.0043	1.0003	1.0426
10	3.80E-05	3.71E-05	4.45E-05	4.38E-05	0.9775	0.9710	0.9791	0.9940
Mean	**5.75E-05**	**5.23E-05**	**5.16E-05**	**8.01E-05**	**1.0095**	**1.0012**	**1.0053**	**1.0297**
Std	**1.66E-05**	**1.47E-05**	**1.49E-05**	**3.19E-05**	**0.0185**	**0.0198**	**0.0152**	**0.0215**

(i) Signal type T1

Trials	RMS error				Coeff of fit			
	N1	N2	N3	N4	N1	N2	N3	N4
1	4.20E-05	3.10E-05	2.53E-05	2.31E-05	1.0693	1.0639	1.0573	1.0479
2	2.47E-05	2.02E-05	1.78E-05	1.52E-05	1.0446	1.0728	1.0729	1.0256
3	1.83E-05	1.70E-05	1.39E-05	1.18E-05	1.0805	1.0615	1.0490	1.0425
4	2.64E-05	2.87E-05	2.59E-05	2.22E-05	1.0528	1.0489	1.0428	1.0182
5	1.40E-05	1.11E-05	9.62E-06	1.00E-05	1.0140	1.0176	1.0036	0.9575
6	1.94E-05	2.29E-05	1.83E-05	1.61E-05	1.0128	0.9890	0.9861	0.9683
7	1.91E-05	1.70E-05	1.30E-05	1.43E-05	1.0250	1.0212	1.0096	0.9814
8	4.18E-05	3.89E-05	3.71E-05	3.65E-05	0.9892	0.9849	0.9731	0.9572
9	2.67E-05	2.49E-05	2.01E-05	1.60E-05	1.1322	1.1270	1.1066	1.0884
10	3.08E-05	2.32E-05	1.74E-05	2.63E-05	1.1040	1.0873	1.0594	1.0897
Mean	**2.63E-05**	**2.35E-05**	**1.98E-05**	**1.91E-05**	**0.9779**	**0.9688**	**0.9522**	**0.8980**
Std	**9.57E-06**	**7.99E-06**	**7.91E-06**	**7.98E-06**	**0.0728**	**0.0779**	**0.0680**	**0.1211**

(ii) Signal type T2

Table 3 RMS error and coefficient of fit for results of various trials using ANN models *N1* to *N4* – Test 1

Trials	RMS error				Coeff of fit			
	N1	N2	N3	N4	N1	N2	N3	N4
1	1.89E-04	1.86E-04	1.40E-04	6.14E-05	0.8357	0.8376	0.8610	0.9146
2	8.38E-05	7.51E-05	7.47E-05	7.44E-05	0.8662	0.8759	0.8824	0.8869
3	2.95E-05	2.32E-05	2.50E-05	2.37E-05	0.9073	0.9148	0.9120	0.9306
4	3.63E-05	3.69E-05	4.22E-05	5.46E-05	0.9372	0.9255	0.9560	0.9668
5	9.93E-05	1.02E-04	7.41E-05	8.13E-05	0.9529	0.9857	0.9791	1.0108
6	3.16E-05	2.89E-05	2.47E-05	2.07E-05	0.8942	0.8981	0.9087	0.9275
7	3.03E-05	2.50E-05	2.14E-05	2.38E-05	0.9392	0.9422	0.9455	0.9851
8	2.99E-05	3.71E-05	3.26E-05	5.66E-05	0.9363	0.9256	0.9375	0.9787
9	4.34E-05	4.10E-05	3.29E-05	1.09E-04	0.9012	0.9035	0.9307	1.0116
10	4.57E-05	4.83E-05	4.11E-05	3.57E-05	0.8953	0.8883	0.9128	0.9230
Mean	**6.19E-05**	**6.03E-05**	**5.08E-05**	**5.42E-05**	**0.9066**	**0.9097**	**0.9226**	**0.9536**
Std	**5.08E-05**	**5.06E-05**	**3.66E-05**	**2.9E-05**	**0.0365**	**0.0399**	**0.0349**	**0.0429**

(iii) Signal type T3

Trials	RMS error				Coeff of fit			
	N1	N2	N3	N4	N1	N2	N3	N4
1	1.64E-03	7.01E-04	8.64E-04	1.70E-03	0.9030	0.8994	0.8643	0.9374
2	9.83E-05	9.88E-05	7.05E-05	1.01E-04	0.9217	0.9461	0.9530	0.9792
3	7.42E-04	2.85E-04	3.93E-04	7.35E-04	1.0835	1.0086	1.0713	1.0611
4	2.77E-04	2.33E-04	1.92E-04	2.09E-04	0.9418	0.9208	0.9338	0.9727
5	2.81E-04	2.99E-04	3.43E-04	7.45E-04	1.0075	1.0133	1.0431	1.0804
6	6.65E-05	7.11E-05	5.87E-05	5.65E-05	0.9526	0.9573	0.9450	0.9637
7	1.38E-03	5.43E-04	6.43E-04	8.55E-04	0.9597	0.9407	0.9029	0.9440
8	4.79E-04	2.41E-04	2.38E-04	3.01E-04	1.0320	0.9594	0.8972	0.8903
9	1.25E-03	7.06E-04	7.19E-04	1.66E-03	1.0023	0.9843	0.9811	1.0184
10	2.12E-04	6.62E-05	1.02E-04	1.10E-04	1.0633	1.0431	1.0387	1.0384
Mean	**6.42E-04**	**3.24E-04**	**3.62E-04**	**6.47E-04**	**0.9867**	**0.9673**	**0.9630**	**0.9886**
Std	**5.78E-04**	**2.44E-04**	**2.88E-04**	**6.18E-04**	**0.0606**	**0.0447**	**0.0693**	**0.0599**

(iv) Signal type T4

Table 3 RMS error and coefficient of fit for results of various trials using ANN models *N1* to *N4* – Test 1

Trials	RMS error				Coeff of fit			
	N1	N2	N3	N4	N1	N2	N3	N4
1	3.58E-05	3.91E-05	3.91E-05	3.89E-05	0.9967	0.9936	1.0153	1.0380
2	4.95E-05	3.99E-05	4.70E-05	4.40E-05	1.0066	1.0022	1.0088	1.0232
3	3.80E-05	3.70E-05	3.72E-05	3.79E-05	0.9843	0.9822	0.9821	1.0044
4	9.79E-05	7.08E-05	9.98E-05	1.00E-04	1.0460	1.0394	1.0499	1.0637
5	1.00E-04	1.20E-04	1.06E-04	7.57E-05	0.9425	0.9279	0.9326	0.9590
6	6.47E-05	3.28E-05	3.96E-05	6.01E-05	1.0164	1.0162	1.0241	1.0344
7	4.56E-05	3.70E-05	3.61E-05	4.42E-05	1.0165	1.0020	0.9983	1.0039
8	2.58E-05	2.24E-05	2.46E-05	2.74E-05	1.0095	0.9965	1.0082	1.0354
9	4.07E-05	5.82E-05	5.67E-05	3.80E-05	0.9842	0.9610	0.9773	1.0083
10	4.77E-05	4.75E-05	5.05E-05	5.65E-05	1.0199	1.0006	1.0045	1.0017
Mean	**5.46E-05**	**5.05E-05**	**5.37E-05**	**5.23E-05**	**1.0022**	**0.9921**	**1.0001**	**1.0172**
Std	**2.55E-05**	**2.79E-05**	**2.75E-05**	**2.18E-05**	**0.0278**	**0.0304**	**0.0314**	**0.0285**

(i) Signal type T1

Trials	RMS error				Coeff of fit			
	N1	N2	N3	N4	N1	N2	N3	N4
1	2.73E-05	2.66E-05	1.95E-05	1.60E-05	1.0470	1.0214	1.0144	1.0113
2	2.09E-05	2.32E-05	1.93E-05	1.36E-05	1.0258	1.0359	1.0110	0.9897
3	1.30E-05	1.05E-05	8.72E-06	1.06E-05	1.0975	1.0838	1.0664	1.0827
4	2.04E-05	2.07E-05	1.73E-05	1.85E-05	0.9853	0.9948	0.9840	0.9693
5	2.98E-05	2.81E-05	2.57E-05	2.13E-05	1.0214	0.9958	0.9866	0.9951
6	2.16E-05	1.46E-05	1.22E-05	1.28E-05	1.0672	1.0359	1.0250	1.0115
7	2.26E-05	1.80E-05	1.35E-05	1.97E-05	1.0744	1.0549	1.0295	1.0304
8	1.38E-05	1.34E-05	1.26E-05	1.25E-05	1.0303	1.0488	1.0380	0.9878
9	2.46E-05	2.28E-05	2.11E-05	1.55E-05	1.0880	1.0725	1.0625	1.0395
10	3.56E-05	2.76E-05	2.54E-05	2.46E-05	1.0919	1.0774	1.0654	1.0509
Mean	**2.30E-05**	**2.05E-05**	**1.75E-05**	**1.65E-05**	**1.0529**	**1.0421**	**1.0283**	**1.0168**
Std	**6.88E-06**	**6.23E-06**	**5.73E-06**	**4.45E-06**	**0.0369**	**0.0316**	**0.0304**	**0.0343**

(ii) Signal type T2

Table 4 RMS error and coefficient of fit for results of various trials using ANN models *N1* to *N4* – Test 2

Trials	RMS error				Coeff of fit			
	N1	N2	N3	N4	N1	N2	N3	N4
1	1.89E-04	1.86E-04	1.40E-04	6.14E-05	0.8357	0.8376	0.8610	0.9146
2	8.38E-05	7.51E-05	7.47E-05	7.44E-05	0.8662	0.8759	0.8824	0.8869
3	2.95E-05	2.32E-05	2.50E-05	2.37E-05	0.9073	0.9148	0.9120	0.9306
4	3.63E-05	3.69E-05	4.22E-05	5.46E-05	0.9372	0.9255	0.9560	0.9668
5	9.93E-05	1.02E-04	7.41E-05	8.13E-05	0.9529	0.9857	0.9791	1.0108
6	3.16E-05	2.89E-05	2.47E-05	2.07E-05	0.8942	0.8981	0.9087	0.9275
7	3.03E-05	2.50E-05	2.14E-05	2.38E-05	0.9392	0.9422	0.9455	0.9851
8	2.99E-05	3.71E-05	3.26E-05	5.66E-05	0.9363	0.9256	0.9375	0.9787
9	4.34E-05	4.10E-05	3.29E-05	1.09E-04	0.9012	0.9035	0.9307	1.0116
10	4.57E-05	4.83E-05	4.11E-05	3.57E-05	0.8953	0.8883	0.9128	0.9230
Mean	**6.19E-05**	**6.03E-05**	**5.08E-05**	**5.42E-05**	**0.9066**	**0.9097**	**0.9226**	**0.9536**
Std	**5.08E-05**	**5.06E-05**	**3.66E-05**	**2.9E-05**	**0.0365**	**0.0399**	**0.0349**	**0.0429**

(iii) Signal type T3

Trials	RMS error				Coeff of fit			
	N1	N2	N3	N4	N1	N2	N3	N4
1	1.01E-04	6.57E-05	6.19E-05	7.01E-05	0.9854	0.9497	0.9485	0.9975
2	2.91E-04	3.08E-04	1.79E-04	3.04E-04	1.0134	0.9928	0.9767	0.9966
3	9.62E-04	4.70E-04	5.93E-04	9.03E-04	1.0078	0.9743	0.9666	0.9973
4	2.60E-04	2.85E-04	3.19E-04	7.04E-04	1.0193	0.9892	1.0274	1.0581
5	2.57E-04	8.97E-05	2.38E-04	8.37E-04	0.9798	0.9383	0.9326	1.0358
6	3.05E-04	1.35E-04	1.07E-04	1.21E-03	1.0007	0.9212	0.9606	1.1563
7	7.19E-05	8.36E-05	1.15E-04	1.50E-04	0.9465	0.9368	0.9437	0.8967
8	8.93E-04	4.09E-04	4.10E-04	1.19E-03	1.0185	0.9243	1.0025	1.0825
9	2.74E-04	1.64E-04	1.13E-04	6.47E-04	0.9781	0.9184	0.9772	1.0996
10	2.16E-04	1.28E-04	1.85E-04	2.74E-04	0.9489	0.9696	0.9596	0.9491
Mean	**3.63E-04**	**2.14E-04**	**2.32E-04**	**6.28E-04**	**0.9898**	**0.9515**	**0.9695**	**1.0269**
Std	**3.08E-04**	**0.000145**	**0.000166**	**0.000414**	**0.0269**	**0.0281**	**0.0283**	**0.0759**

(iv) Signal type T4

Table 4 RMS error and coefficient of fit for results of various trials using ANN models *N1* to *N4* – Test 2

Run	Run time (s)				
	N1	N2	N3	N4	RFC
1	10.54	10.44	11.29	11.54	40.09
2	10.57	10.60	11.71	12.88	40.12
3	10.52	10.58	10.84	11.86	40.13
Average	10.54	10.54	11.28	12.09	40.11

Table 5 Performance indicators using tic toc run time in MATLAB for different ANN network types and rainflow counting method. Number of signals analysed in each run was 10,000.